AGU PUBLICATIONS

Water Resources Research

RESEARCH ARTICLE
10.1002/2016WR019579

Key Points:
- Velocity profiles deviate from logarithmic in the roughness layer and are self-similar
- Energetic subsurface flow through a cobble bed affects flow velocities far above the bed
- Grain drag alone can account for high flow resistance observed in mountain streams

Supporting Information:
- Supporting Information S1

Correspondence to:
M. P. Lamb,
mpl@gps.caltech.edu

Citation:
Lamb, M. P., F. Brun, and B. M. Fuller (2017), Hydrodynamics of steep streams with planar coarse-grained beds: Turbulence, flow resistance, and implications for sediment transport, *Water Resour. Res.*, *53*, doi:10.1002/2016WR019579.

Received 28 JUL 2016
Accepted 22 FEB 2017
Accepted article online 3 MAR 2017

Hydrodynamics of steep streams with planar coarse-grained beds: Turbulence, flow resistance, and implications for sediment transport

Michael P. Lamb[1], Fanny Brun[1], and Brian M. Fuller[1]

[1]Division of Geological and Planetary Sciences, California Institute of Technology, Pasadena, California, USA

Abstract The hydraulics of steep mountain streams differ from lower gradient rivers due to shallow and rough flows, energetic subsurface flow, and macro-scale form drag from immobile boulders and channel and bed forms. Heightened flow resistance and reduced sediment transport rates in steep streams are commonly attributed to macro-scale form drag; however, little work has explored steep river hydrodynamics in the absence of complex bed geometries. Here we present theory for the vertical structure of flow velocity in steep streams with planar, rough beds that couples surface and subsurface flow. We test it against flume experiments using a bed of fixed cobbles over a wide range of bed slopes (0.4–30%). Experimental flows have a nearly logarithmic velocity profile far above the bed; flow velocity decreases less than logarithmically toward the bed and is nonzero at the bed surface. Velocity profiles match theory derived using a hybrid eddy viscosity model, in which the mixing length is a function of height above the bed and bed roughness. Subsurface flow velocities are large (>1 m/s) and follow a modified Darcy-Brinkman-Forchheimer relation that accounts for channel slope and shear from overlying surface flow. Near-bed turbulent fluctuations decrease for shallow, rough flows and scale with the depth-averaged flow velocity rather than bed shear velocity. Flow resistance for rough, planar beds closely matches observations in natural steep streams despite the lack of bed forms or channel forms in the experiments, suggesting that macro-scale form drag is smaller than commonly assumed in stress-partitioning models for sediment transport.

1. Introduction

Steep, coarse-bedded channels dominate the drainage network in mountainous terrain, and understanding their hydraulics is important for flood mitigation, habitat classification and restoration, and sediment transport in engineering and geomorphology [*Buffington et al.*, 2004; *Yager et al.*, 2007; *Rickenmann and Recking*, 2011]. Despite more than a century of work on the hydraulics of rivers, most of this effort has been devoted to moderate to low gradient rivers ($S < 0.01$, where S is the bed slope) and significant uncertainty exists for steep streams ($0.01 < S < 0.3$) [*Scheingross et al.*, 2013; *Heimann et al.*, 2015; *Prancevic and Lamb*, 2015b; *Schneider et al.*, 2015a]. Observations suggest that the hydraulics of steep streams differ in important ways from better studied lower gradient rivers. For example, friction factors (i.e., flow resistance coefficients), which relate the bed shear stress to the depth-averaged flow velocity (i.e., $C_f = u_*^2/U^2$ where u_* is the bed shear velocity and U is the depth-averaged flow velocity), are much greater in steep rivers than predicted by empirical models developed for lower gradient rivers [*Bathurst*, 1985; *Aberle and Smart*, 2003; *Ferro*, 2003; *Wilcox et al.*, 2006; *Ferguson*, 2007; *Rickenmann and Recking*, 2011]. The vertical profile of flow velocity can deviate from the classic logarithmic profile known for lower gradient rivers [*Wiberg and Smith*, 1991; *Byrd et al.*, 2000; *Wohl and Thompson*, 2000; *Nikora et al.*, 2004], and the intensity of near-bed velocity fluctuations (σ_u/u_* where σ_u is the root-mean-square of flow velocity fluctuations in the downstream direction) due to turbulence is smaller in shallow, rough flows [*Wang et al.*, 1993; *Carollo et al.*, 2005; *Lamb et al.*, 2008]. Furthermore, semiempirical models for initial sediment motion and bed load flux developed for lower gradient rivers substantially overestimate sediment transport in steep rivers [*Lenzi et al.*, 1999; *Rickenmann*, 2001; *Mueller et al.*, 2005; *Yager et al.*, 2012].

One of the leading ideas to explain these observations is that hydraulics and sediment transport are different in steep streams, as compared with lower gradient rivers, because of the presence of rarely mobile (or

immobile) large boulders, particle clusters, and bed forms or channel forms such as pool-riffle or step-pool sequences [*Buffington and Montgomery*, 1999; *Millar*, 1999; *Wilcox et al*., 2006; *Yager et al*., 2007; *Nitsche et al*., 2011; *Ferguson*, 2012; *Schneider et al*., 2015b]. Interlocking of boulders in steps and other bed structuring can stabilize sediment and reduce transport rates [*Church et al*., 1998; *Zimmermann et al*., 2010]. These bed forms also create a series of overspills and pools that affect the development of a logarithmic boundary layer and may limit the scale and intensity of turbulent eddies [*Wohl and Thompson*, 2000; *Zimmermann*, 2010]. Perhaps more importantly, form drag on immobile boulders and boulder steps (herein referred to as morphologic form drag to distinguish it from grain drag on the mobile bed sediment) is often argued to be the primary mechanism to slow the flow thereby increasing the friction factor [*Buffington and Montgomery*, 1999; *Aberle and Smart*, 2003; *Wilcox et al*., 2006; *Ferguson*, 2012]. Morphologic form drag is also thought to reduce the bed stress available to drive sediment transport, and therefore may explain heightened critical Shields numbers for initial sediment motion [*Mueller et al*., 2005; *Recking*, 2009; *Ferguson*, 2012] and reduced sediment transport rates [*Rickenmann*, 2001; *Yager et al*., 2007; *Schneider et al*., 2015b] in steep streams.

In order to empirically assess the influence of larger boulders and bed forms on flow hydraulics and sediment transport, it is typical to compare observations from rivers or flumes with bed forms to "base cases" without bed forms, while holding all other parameters constant. This comparison is the basis of classic theory for linear stress partitioning in rivers where the total frictional stress can be computed as the sum of drag on the bed sediment, banks, and morphologic form drag due to bed forms and other macro-scale roughness [*Einstein and Barbarossa*, 1952]. Similar concepts have been adopted for linear partitioning of friction factors [*Millar*, 1999; *Wilcox et al*., 2006; *Rickenmann and Recking*, 2011]. Similarly, the influence of bed forms and large boulders on the vertical structure of flow velocity and turbulence is often assessed by comparison with expectations (e.g., logarithmic profile) developed from planar beds [*Wiberg and Smith*, 1991; *Byrd et al*., 2000].

Decades of measurements of flow hydraulics for planar, rough beds have provided this bed form-free base case in low gradient rivers, building on the work of *Nikuradse* [1933], which allows for quantitative assessment of the role of bed forms in momentum conservation, flow resistance, the structure of the velocity profile, and sediment transport [*Meyer-Peter and Müller*, 1948; *Engelund and Hansen*, 1967; *Parker and Peterson*, 1980]. For example, the friction coefficient is often related to flow depth, h, and bed roughness height, k_s, using a Manning-Strickler relation

$$C_f \equiv \frac{u_*^2}{U^2} = a\left(\frac{h}{k_s}\right)^b \tag{1}$$

in which $a = 0.015$ and $b = -1/3$ are often used successfully for low gradient gravel bed rivers with planar beds [*Parker*, 1991]. However, similar, well-accepted theories for base-case flow resistance (i.e., for planar, rough beds that lack larger-scale morphologic form drag) are not available for steep streams. This knowledge gap exists because few natural high-gradient streams exist without the complicating issues of bed forms and immobile boulders [*Rickenmann*, 2012; *Yager et al*., 2012], and most flume experiments to date have focused on lower gradient rivers, or have complicating effects related to bed forms or channel forms [*Crowe*, 2002; *Zimmermann et al*., 2010] and sediment transport [*Bathurst et al*., 1987; *Recking et al*., 2008a, 2008b]. Nonetheless, the few experimental studies aimed at steep, coarse-grained rivers with planar (or nearly planar) beds report C_f values typically much larger than predicted by equation (1), especially for cases with large relative roughness (e.g., $k_s/h > 0.2$) [*Mizuyama*, 1977; *Bathurst et al*., 1981; *Cao*, 1985; *Rice et al*., 1998; *Recking et al*., 2008a].

The lack of a well-accepted baseline for steep streams has led many workers to apply relations developed for lower gradient rivers, like equation (1), to steep streams. For example, several studies compare field and flume measurements of hydraulics and sediment transport in natural steep streams that contain the complicating effects of immobile boulders and bed forms to empirical relationships developed for low gradient rivers with planar beds, and attribute the often significant differences to effects that arise from the presence of form drag on immobile boulders or step-pool bed forms [*Rickenmann*, 2001; *Nitsche et al*., 2011; *Ferguson*, 2012; *Yager et al*., 2012]. An additional possibility, however, is that the hydraulics of steep streams differ from lower gradient rivers even for planar, rough beds that lack bed forms and other sources of macro-scale form drag.

There are several reasons to expect that empirical relationships developed for low gradient planar-bed rivers may not apply to steep streams, even for cases without bed forms or channel forms, grain interlocking,

or large immobile boulders. Steep streams tend to have small flow depths relative to the gravel, cobbles, or boulders that compose the mobile part of the river bed, even at bankfull stages, such that the so-called "roughness layer" [*Nikora et al*., 2001] makes up a substantial portion of the flow [*Bathurst*, 1985; *Recking*, 2009]. Moreover, shallow flows on steep slopes with planar, rough beds can have Froude numbers that approach or exceed unity, resulting in highly three-dimensional flow that spills over grain tops [*Zimmermann*, 2010], standing and breaking waves [*Flammer et al*., 1970; *Lawrence*, 2000] and significant aeration [*Straub and Lamb*, 1956; *Valle and Pasternack*, 2006]. On steep slopes, near-bed flow velocities can be high even for shallow flow, which combined with coarse, permeable bed sediment, results in large bed roughness Reynolds numbers (i.e., $\mathrm{Re}_{k_s}=u_* k_s/\nu > 10^3$, where k_s is the characteristic bed roughness height and ν is the kinematic viscosity) and fully turbulent wakes behind particles. In addition, the combination of steep bed gradients and coarse bed material can produce significant subsurface flow through the bed, which may be non-Darcian or turbulent [*Packman et al*., 2004; *Manes et al*., 2011a].

There is a need to develop and test theory for the hydraulics of steep streams with planar, rough beds in the absence of bed forms and large boulders, similar to what has been done for lower gradient rivers and pipe flow, to form a base case that can be compared with more complex bed and channel geometries in natural rivers. To this end, we review previous work on the hydraulics of coupled surface and subsurface flows in section 2. This work is used as a basis for a new 1-D flow velocity model in steep rivers with planar, rough beds presented in section 3. Section 4 describes methods for flume experiments where we measured vertical profiles of flow velocity and turbulence over a planar cobble bed and across a wide range of channel gradients and water discharges. Section 5 reports the experimental results and comparison with our model. Section 6 discusses the implications of our results for stress partitioning and the role of bed forms in flow resistance and sediment transport in steep streams.

2. Background and Problem Conceptualization

It is useful to conceptualize the hydraulics of mountain rivers as composed of surface flow ($z > 0$) and subsurface flow ($z < 0$) with the boundary between the two representing the average bed elevation (Figure 1). Following *Nikora et al*. [2001], the surface flow can be divided into three main layers: a roughness layer, logarithmic layer, and an outer layer. In low gradient rivers, the roughness layer is typically a small part of the flow depth, and often the outer layer is neglected, so that workers tend to use the well-known log law for turbulent boundary layers

$$\frac{\overline{u}(z)}{u_*}=\frac{1}{\kappa}\ln\left(\frac{z}{z_0}\right)=\frac{1}{\kappa}\ln\left(\frac{30z}{k_s}\right) \tag{2}$$

where $\overline{u}(z)$ is the downstream velocity averaged in time over turbulence and laterally in space over variability in local bed roughness, z is the distance above the bed in the direction perpendicular to the bed, κ is von Karman's constant of 0.41, and $z_0 = k_s/30$ for hydraulically rough flow [*Schlichting*, 1979]. In practice, the depth-averaged version of equation (2) is often approximated as a power law resulting in equation (1).

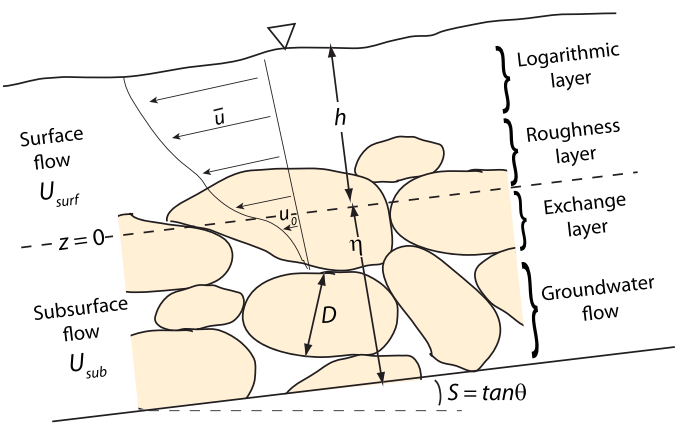

Figure 1. Schematic of zones of flow for the surface ($z > 0$) and subsurface ($z < 0$) over a rough, permeable bed. The bed slope angle is θ, h is the average flow depth, η is the average bed thickness, D is the sediment intermediate diameter, $\bar{u}$ is the downstream flow velocity averaged over turbulence, and u_0 is $\bar{u}$ at $z = 0$.

For flows with high relative roughness (i.e., large k_s/h), the roughness layer cannot be neglected. The roughness layer is a region where flow velocities and stresses are strongly affected by blockage and form drag induced from the grain roughness [*Nowell and Church*, 1979; *Dittrich and Koll*, 1997; *Lawrence*, 1997; *Gioia and Chakraborty*, 2006] (Figure 1). *Wiberg and Smith* [1991]

solved for the effect of grain drag on the momentum balance in the roughness layer and showed that flow should deviate from logarithmic in the roughness layer. *Nikora et al*. [2001] suggested both a linear and exponential velocity profile for the roughness layer based on different scaling arguments of the double-averaged equations of motion, and both may be valid depending on the spacing of the roughness elements [*Coleman et al*., 2007]. To account for reduced sediment transport in very shallow flows, *Lamb et al*. [2008] derived a model within the roughness layer that predicted a linear profile for deep flows, and a quadratic profile with lower velocities for shallow flows. *Recking* [2009] proposed vertically uniform flow velocity in the roughness layer, and a velocity magnitude within the roughness layer that decreases for shallow, rough flows by comparison to bulk friction factors.

The subsurface layer consists of flow through pores between particles (Figure 1). Although the subsurface flow is often considered negligible in rivers, it is more important in steep rivers where large head gradients can drive fast flow through permeable, coarse-grained beds [*Packman et al*., 2004]. Following *Nepf and Vivoni* [2000] and *Manes et al*. [2012], we conceptualize the subsurface flow consisting of a lower layer of groundwater flow and an upper "exchange layer." Flow in the exchange layer differs from that in the groundwater layer because here shear and turbulence from the surface flow above drive enhanced subsurface flow and mixing [*Chan et al*., 2007; *Rathnayake and Izumi*, 2009]. For example, *Packman et al*. [2004] showed that diffusion into the bed is a function of the overlying flow, turbulence, momentum transfer, and pore geometry. Exchange layer depth is expected to scale with a drag length parametrized by the aerial density of roughness elements and a drag coefficient [*Nepf et al*., 2007], which likely scales with grain diameter for a gravel bed [*Manes et al*., 2012]. Similar to classical theory for flow through porous media, flow in the groundwater layer is driven by a hydraulic head gradient, which for flow through a channel bed is on average proportional to the bed slope. Subsurface flow is typically modeled using Darcy's law. However, in coarse-grained rivers subsurface flow is likely to violate Darcy's law and in cases be fully turbulent and may be better represented by Forchheimer's equation [*Chaudhary et al*., 2011; *Manes et al*., 2012].

Few studies have attempted to couple turbulent surface flow with a roughness layer and non-Darcian subsurface flow. *Beavers and Joseph* [1967] found an analytical solution for the case of coupled laminar surface flow and Darcian subsurface flow. Others have extended this analysis to turbulent surface flow, but still with Darcian subsurface flow [*Manes et al*., 2011b; *Battiato*, 2012]. Studies that do include non-Darcian subsurface flow typically do not include a roughness layer [*Vafai and Kim*, 1990; *Zhou and Mendoza*, 1993; *Chan et al*., 2007]. *Katul et al*. [2002] proposed a hyperbolic tangent function to describe flow velocity within and slightly above the roughness layer. The function predicts that the velocity profile is symmetric about the roughness layer, which is unlikely to hold far from the bed [*White and Nepf*, 2008].

Probably the most detailed work in coupled surface and subsurface flows has been done for flow through submerged vegetation or for wind over a canopy [*Raupach et al*., 1991; *Nepf and Vivoni*, 2000; *Nepf*, 2012]. For example, *Defina and Bixio* [2005] found good support for the two layer model of *Klopstra et al*. [1997] that couples form drag dominated subsurface flow below the canopy with a logarithmic profile above. Similar models have been derived for depth-averaged flow above and within cylindrical vegetation stems [*Huthoff et al*., 2007; *Konings et al*., 2012]. While similar in some respects, there are several differences that make application of models for flow over vegetation to steep, rough river beds uncertain. First, since vegetation is typically conceptualized as flexible near-vertical columns, the location of the boundary between the surface and subsurface flow is unclear for vegetation, and thus the roughness layer and subsurface layer are typically treated as one layer. In this case, a fit parameter, the so-called zero displacement height, must be used to define the location of the boundary condition $z = z_0$ that is needed for the upper log layer [*Raupach et al*., 1991]. In contrast, for a gravel bed, the boundary between surface and subsurface flow is more easily defined as the average bed elevation, and the porosity decreases in a predictable way from the particle tops into the bed [e.g., *Nikora et al*., 2001]. Second, the deformability of vegetation results in flow dynamics that do not exist for a rigid rough bed [*Ghisalberti and Nepf*, 2009]. Finally, flow over vegetation is typically considered for cases with small (or zero) bed gradient, such that all of the potential changes in surface flow hydraulics discussed above for steep rivers may not be present for vegetated flows. In addition, subsurface flow through vegetation on low (or zero) bed gradients is dominated by shear and mixing from the overriding surface flow [*Nepf and Vivoni*, 2000]. In mountain streams, on the other hand, head gradients due to the steep bed slope can drive significant subsurface flow independent of surface flow.

3. Model Development

Here we build on previous work and derive a new 1-D model for coupled subsurface and surface flow centered on application to steep rivers with rough, planar beds. The model is implicitly assumed to represent flow velocity averaged in time over turbulence and laterally in space over variability in local grain-scale bed roughness. First, the surface flow model is derived based on a mixing-length argument. Then the surface flow is coupled to a model for non-Darcian subsurface flow driven by both the bed slope and shear from the overriding surface flow. Finally the result is depth averaged to derive the friction factor.

3.1. Hybrid Mixing-Length Model

Our approach to the surface flow is similar to others who have used a mixing length to derive the vertical velocity profile in the roughness layer [*Mizuyama*, 1977; *Schlichting*, 1979; *Wiberg and Smith*, 1987a; *Nelson et al*., 1991; *Wiberg and Smith*, 1991; *Lawrence*, 1997; *Nikora et al*., 2001; *Lamb et al*., 2008]. We follow *Christensen* [1972] and propose a mixing-length model that is intended to work seamlessly across the roughness layer and into the logarithmic layer.

The vertical structure of flow in turbulent open channel flow can be approximated using the Boussinesq eddy viscosity approach

$$\tau(z)=\rho u_*^2\left(1-\frac{z}{h}\right)=\rho\varepsilon d\overline{u}/dz \tag{3}$$

in which $\tau(z)$ is the shear stress, $u_* \equiv \sqrt{\tau(z=0)/\rho}$ is the bed shear velocity, h is the flow depth and ρ is fluid density. Following Prandtl's hypothesis, the eddy viscosity, ε, can be approximated as the product of local turbulence velocity (u_t) and length (L) scales, i.e.,

$$\varepsilon=u_*\left(1-\frac{z}{h}\right)L \tag{4}$$

in which the turbulent velocity is assumed to decrease linearly with distance above the bed (i.e., $u_t=u_*(1-z/h)$). If eddy size is set to be proportional to distance from the bed,

$$L=\kappa z \tag{5}$$

then equations (3)–(5) can be combined and integrated to yield the well-known log law for turbulent boundary layers (equation (2)).

Within the roughness layer (Figure 1), flow velocity can deviate substantially from equation (2). For flows with large relative roughness (k_s/h), turbulent mixing is dominated by wakes shed from roughness elements, and therefore the mixing length within the roughness layer might be better described by

$$L=\alpha_1 k_s \tag{6}$$

where α_1 is a constant of proportionality that is likely less than unity [*Schlichting*, 1979; *Wiberg and Smith*, 1987a; *Nelson et al*., 1991; *Wiberg and Smith*, 1991]. For grain roughness of interest here, $k_s \approx 2.5D_{84}$ [e.g., *Kamphuis*, 1974] (Figure 2b). Equation (6) has also been proposed for mixing within vegetation [*Rowinski and Kubrak*, 2002] and confirmed by experiments [*Ghisalberti and Nepf*, 2009]. *Lamb et al*. [2008] used equations (3), (4), and (6) to derive a velocity profile model within the roughness layer that varies from linear for deep flows to parabolic for shallow flows; however, their model does not apply to the flow above the roughness layer (i.e., $z > k_s$), and introduces an unrealistic discontinuity in the velocity profile gradient at the top of the roughness layer.

To derive an approximate velocity profile that is valid for both the roughness layer and the logarithmic layer (Figure 1), and for both shallow ($h < k_s$) and deep ($h > k_s$) flows, here we use a hybrid mixing-length model in which the length scale of turbulent mixing is controlled by both grain roughness and the distance from the bed, i.e., the sum of equations (5) and (6) [*Christensen*, 1972],

$$L=\kappa z+\alpha_1 k_s \tag{7}$$

Thus, near the bed equation (7) approaches equation (6) and mixing is dominated by grain roughness. Far from the bed ($z > k_s$), equation (7) approaches equation (5) similar to Prandtl's original hypothesis. This approach is somewhat similar to that of *Ferguson* [2007] in that he proposed a model for depth-averaged

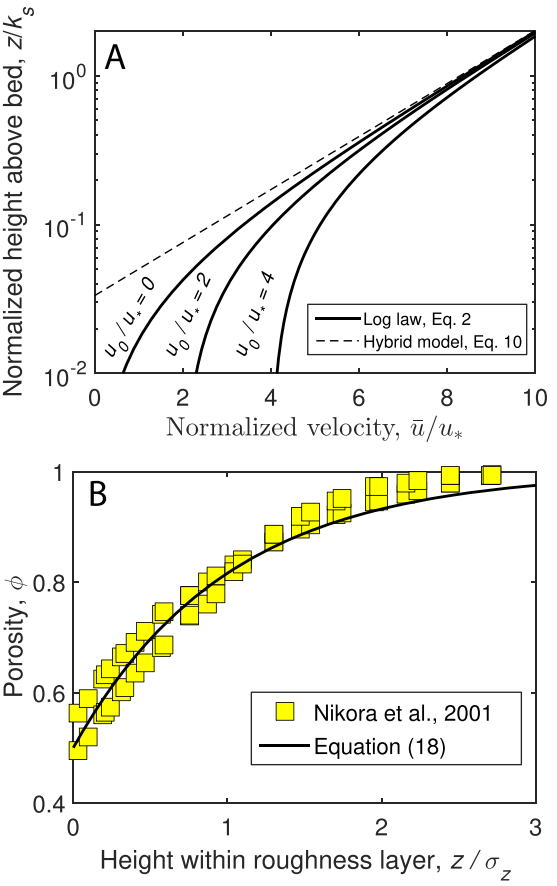

Figure 2. (a) Example velocity profiles predicted by the log law (equation (2)) and the proposed hybrid mixing-length model (equation (10)) for different values of subsurface flow. (b) Porosity within the roughness layer for a gravel bed as presented by *Nikora et al.* [2001, Figure 3] based on a compilation of data from natural rivers and flume experiments, which showed little variation, from *Nikora et al.* [1998]. To generate the points in Figure 2b, we equated the standard deviation of bed elevation from *Nikora et al.* [2001] to $0.875k_s$ based on the analysis of *Nikora et al.* [1998]. Our best fit curve is equation (18).

velocity (e.g., equation (2)) that works seamlessly across shallow and deep flows, but it was not derived in terms of a vertical velocity profile. Equations (3), (4), and (7) can be combined and integrated to yield

$$\frac{\overline{u}(z)-u_0}{u_*}=\frac{1}{\kappa}\ln\left(1+\frac{\kappa z}{\alpha_1 k_s}\right) \tag{8}$$

in which the boundary condition $\overline{u}(z=0)=u_0$ has been applied, where u_0 is a seepage velocity at the bed surface that is likely nonzero in permeable gravel beds on steep slopes (Figure 1). Note that the boundary condition $\overline{u}(z=z_0)=0$ as typically applied in derivation of the log law is not necessary here because, unlike the standard derivation, there is not a singularity at $z=0$ in equation (8). Equation (8) should converge to the typical log law for deep flow, and therefore equations (2) and (8) can be combined to solve for the unknown coefficient in the limit of $z \gg k_s$,

$$\alpha_1=\frac{\kappa}{30}\exp\left(\kappa\frac{u_0}{u_*}\right) \tag{9}$$

For the case of an impermeable bed, $u_0=0$ and equation (9) reduces to $\alpha_1=\frac{\kappa}{30}=0.014$. Combination of equations (8) and (9) results in a prediction for the velocity profile both within and above the roughness layer

$$\frac{\overline{u}(z)-u_0}{u_*}=\frac{1}{\kappa}\ln\left(1+\frac{30z}{k_s}\exp\left(-\kappa\frac{u_0}{u_*}\right)\right) \tag{10}$$

For the case of an impermeable bed, equation (10) reduces to

$$\frac{\overline{u}(z)}{u_*}=\frac{1}{\kappa}\ln\left(1+\frac{30z}{k_s}\right) \tag{11}$$

Equation (11), like the original log law, is a simple function of height above the bed, and it converges with the log law for deep flow ($z \gg k_s$) (Figure 2a). The two models differ, however, near the bed where equation (11) predicts overall greater velocities than equation (2), and finite velocities in the region of $0<z<k_s/30$ rather than zero velocity as in equation (2). Equation (11) is similar to the zero-plane displacement concept often used in flow over vegetation to specify a virtual origin of the bed [*Raupach et al.*, 1991]. Here we find that the displacement height must be k_s for equation (10) to converge to the log-profile above the roughness layer. Unlike the model of *Lamb et al.* [2008], the hybrid mixing-length model proposed here applies both above and within the roughness layer and predicts a smooth velocity profile across the entire flow depth (Figure 2a). In addition, Figure 2a also shows that the near-bed flow velocities predicted by equation (10) increase with increasing subsurface flow velocities, u_0, while still converging with the standard log law higher up in the water column. In the next section, we formulate a model for subsurface flow velocity, owing to the potential importance of subsurface flow in altering the surface flow velocity profile through u_0.

3.2. Subsurface Flow Model

Subsurface flow at scales larger than the pore scale and for large subsurface Reynolds numbers can be modeled using the Darcy-Forchheimer-Brinkman equation, which for steady, uniform, unconfined flow in 1-D is given by [*Bear*, 1972]

$$-S=\frac{1}{\rho g}\frac{d\tau}{dz}-\frac{u}{K}-F^{*}u^{2} \tag{12}$$

in which $K=\frac{\rho g k}{\mu}$ is the hydraulic conductivity, $F^{*}=\frac{F\phi_{sub}}{g\sqrt{k}}$, g is the acceleration due to gravity, $-S$ is the head gradient (which in our case is the negative of bed slope), μ is the fluid viscosity, k is the permeability, F is the Forchheimer coefficient, and ϕ_{sub} is the porosity in the subsurface. On the right-hand side of equation (12), the first term is the Brinkman term that accounts for fluid shear stress gradients, the second term is the Darcy term, and the third term is the Forchheimer term that is necessary for large pore-Reynolds numbers for flow through gravel and cobbles. If the Brinkman and Forchheimer terms are neglected, equation (12) simplifies to the standard form of Darcy's Law ($-S = -u/K$).

Equation (12) shows that the gradient in fluid shear stress across the bed surface ($z = 0$) must be known to determine u_0. For the case of coupled surface-subsurface flow of concern here, $d\tau/dz$ is nonzero at $z = 0$ due to shear from the overlying surface flow, and is not known a priori. Equation (12) can be rewritten as a second order nonlinear ordinary differential equation using an eddy viscosity closure for τ and solved numerically. However, here we seek a simpler analytical approximation to equation (12).

Surface flows affect the subsurface flow velocity, shear stress, and turbulence to some level below the bed surface known as the exchange depth $z = -P$ [*Nepf and Vivoni*, 2000; *Ghisalberti*, 2009] (Figure 1), below which $\tau(z \le -P) \approx 0$ at the macropore scale. Depth averaging equation (12) from the bed surface ($z = 0$) to the exchange depth ($z = -P$) and rearranging results in

$$S\left(1+\frac{h}{P}\right)=\frac{U_{sub}}{K}+C_1F^{*}U_{sub}^{2} \tag{13}$$

in which $U_{sub}=\frac{1}{P}\int_{-P}^{0}\bar{u}\,dz$ is the depth-averaged subsurface velocity in the exchange layer of thickness P and $\tau(0)=\tau_b=\rho g h \sin\theta \approx \rho g h S$ for steady and uniform surface flow. To perform the integration analytically in equation (13), we approximate the square of the depth-averaged velocity within the exchange zone as $\frac{1}{P}\int_{-P}^{0}\bar{u}^2dz=C_1U_{sub}^2$ where the value of C_1 depends on the shape of the subsurface velocity profile and is likely order one. For example, if the velocity profile in the exchange layer is linear [*Nikora et al*., 2001] and the deep groundwater flow is negligible, then $C_1 = 2$. If the profile decays exponentially with an e-folding length of P, then $C_1 = 1.4$. Equation (13) can be solved using the quadratic formula,

$$U_{sub}=\frac{1}{2}\sqrt{\left(\frac{1}{C_1KF^{*}}\right)^{2}+\frac{4S}{C_1F^{*}}\left(\frac{h}{P}+1\right)}-\frac{1}{2}\frac{1}{C_1KF^{*}} \tag{14}$$

Finally, we argue that the flow velocity at the bed surface through the grains, u_0, should scale linearly with the depth-averaged flow velocity within the exchange layer, so that

$$u_0=C_2U_{sub}/\phi_{sub} \tag{15}$$

where C_2 is an order one constant that again depends on the shape of the velocity profile within the exchange layer. If the profile is linear and the deep groundwater flow is negligible, then $C_2 = 2$. If the profile is an exponential decay with an e-folding length of P, then $C_2 = 1.6$.

There are no data, to our knowledge, to test equations (14) and (15) for coupled surface and subsurface flow in rivers; however, simpler solutions to equation (14) exist for special cases which yield familiar results. For example, for subsurface flow within submerged vegetation or a tree canopy that is driven entirely by shear from the overlying fluid, $S = 0$ in equation (12), and if the Darcy term is neglected, equation (12) reduces to $F^{*}u^2=\frac{1}{\rho g}\frac{d\tau}{dz}$, which can be integrated across the exchange layer as above, to yield

$$\frac{u_0^2}{u_*^2}=C_2\frac{U_{sub}^2}{u_*^2}=\frac{C_2}{C_1gPF^{*}} \tag{16}$$

Equation (16) is similar to findings for flow over canopies of vegetation [*Huthoff et al*., 2007; *Nepf*, 2012], where the dimensionless coefficient $\frac{C_2}{C_1gPF^{*}}$ has been found to be equal to ~2.6 [*Ghisalberti*, 2009].

3.3. Depth-Averaged Flow and Bulk Friction Factor

To derive the depth-averaged surface flow within the roughness and logarithmic layers (U_{surf}), the product of the flow velocity and porosity can be integrated from zero to the flow depth (h) and normalized by h, that is

$$\frac{U_{surf}}{u_*} = \frac{1}{h}\int_0^h \frac{\bar{u}(z)}{u_*}\phi(z)dz \tag{17}$$

Based on the data of *Nikora et al*. [1998, 2001] for natural and experimental gravel beds, we find that porosity in the roughness layer is well represented by

$$\phi(z) = 1 - 0.5\exp\left(-\frac{z}{\sigma_z}\right) \tag{18}$$

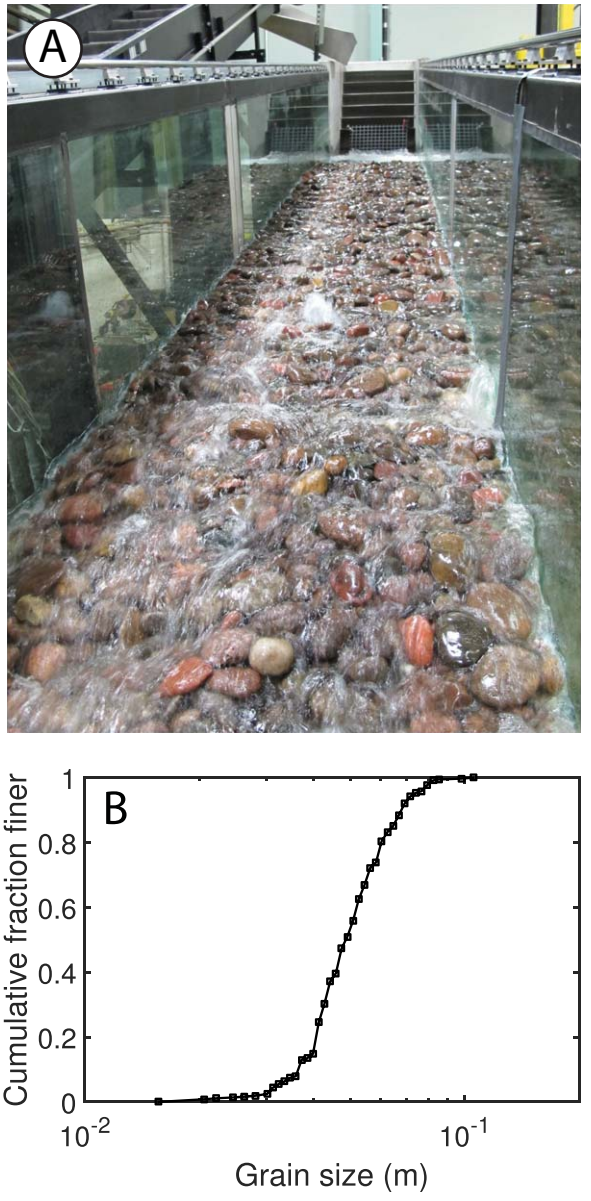

Figure 3. (a) View looking upstream in the flume bed with shallow flow at $S = 0.15$ (Experiment 43; supporting information Table S1). (b) Grain-size distribution for the intermediate diameter of cobbles used in the experiments.

in which σ_z is the standard deviation of elevations, which we set equal to 0.35 D_{50} based on the grain-size distributions presented in *Nikora et al*. [1998]. Equation (18) produces the expected behavior of $\phi = 1$ far above the roughness layer, porosity is reduced within the roughness layer, and $\phi = \phi_{sub} = 0.5$ at $z = 0$. We insert equations (10) and (18) into (17) and integrate using finite differences to find the depth-averaged surface velocity, U_{surf}. The total depth-averaged velocity, U, including surface flow and subsurface flow within the exchange layer is then

$$U = \frac{U_{surf}h + U_{sub}P}{h + P} \tag{19}$$

for the case of negligible deep subsurface flow (e.g., due to filling of pores with fines, or a bedrock boundary), which is the case for our flume experiments. The bulk friction coefficients can now be estimated using $C_{f,total} = u_*^2/U^2$ for the combined surface and subsurface flow, and $C_{f,surf} = u_*^2/U_{surf}^2$ for surface flow alone.

4. Experimental Setup and Methods

Experiments were designed to explore the hydraulics of flow over a rough and planar bed across a wide range of conditions relevant for steep mountain streams. The experiments were carried out in a 15 m long, 1 m wide tilting flume at the California Institute of Technology (Figure 3a). The flume has smooth glass walls, such that wall stresses are negligible, especially for the coarse-bedded, shallow flows of concern here. Fifty-eight experiments were conducted using the same cobble bed and

Table 1. Summary of Experiments

Experiment Set (Number of Experiments)	Bed Slope, S	Discharge, Q (m^3/s)	Subsurface Discharge, Q_{sub}[a] (m^3/s) ($\times 10^{-3}$)	Depth-Averaged Velocity, U_{surf} (m/s)	Flow Depth, h (m)	Subsurface Velocity, u_0 (m/s)	Flow Reynolds Number, Re ($\times 10^4$)	Froude Number, Fr	Relative Roughness, k_s/h	Roughness Reynolds Number, Re_{k_s} ($\times 10^4$)	Shields Number, τ_*
1 (16)	0.004	0.02–0.69	0.43–1.8	0.23–1.39	0.09–0.52	0.16–0.38	2.0–69	0.25– 0.63	0.31–1.85	0.92–2.2	0.004–0.024
2 (17)	0.02	0.01–0.69	1.0–5.2	0.24–2.11	0.03–0.33	0.33–0.82	0.67–69	0.45–1.18	0.49–5.76	1.2–4.0	0.007–0.078
3 (8)	0.08	0.03–0.52	4.9–10.7	0.48–2.67	0.05–0.19	0.57–1.83	2.5–50	0.68–1.96	0.84–3.12	3.2–6.2	0.051–0.19
4 (8)	0.15	0.01–0.51	6.1–15.0	0.15–3.24	0.03–0.16	2.04–2.26	0.4–50	0.29–7.8	1.0–6.03	2.6–7.8	0.051–0.30
5 (9)	0.3	0.007–0.5	9–20.5	0.34–3.69	0.02–0.13		1–48	0.59–3.26	1.23–9.3	3.5–9.6	0.06–0.48

[a]Subsurface discharge was calculated, not measured, using $Q_{sub} = U_{sub}PW$.

varying channel-bed slope ($0.004 < S < 0.3$) and flow discharge ($0.007 < Q < 0.69$ m^3/s) over a wide range of conditions, including cases much steeper than typically investigated (Table 1; Table S1 supporting information). All flows were fully turbulent ($\mathrm{Re} = U_{surf}h/\nu > 10^3$) and Froude numbers ranged from subcritical to supercritical ($0.25 < \mathrm{Fr} < 7.8$, in which $\mathrm{Fr} = U_{surf}/\sqrt{gh}$).

Natural river cobbles with a median grain diameter of $D_{50} = 49$ mm and $D_{84} = 64$ mm (Figure 3) were hand screed to a thickness of about one grain diameter. The sediment size was picked to ensure large roughness Reynolds numbers ($\mathrm{Re}_{k_s} = u_* k_s/\nu > 10^3$; Table 1), consistent with most mountain streams. The cobbles were fixed to the flume floor using a thin coating of epoxy, which did not alter particle sizes, shapes or pore spaces significantly. We fixed the particles to flume floor in order to explore hydraulic conditions that exceed that required to mobilize sediment while preventing bed load transport and the formation of bed forms (e.g., alternating bars or step pools), to maintain the planar, base-case scenario needed for stress partitioning. For example, many of the Shields numbers ($\tau_* = \frac{u_*^2}{RgD_{50}}$, where $R = 1.65$ is the submerged specific density of sediment) in our experiments ($0.004 < \tau_* < 0.48$; Table 1) were near or exceeded the expected threshold of motion [*Lamb et al*., 2008; *Prancevic et al*., 2014].

The flume is equipped with a motorized cart that travels on rails and carries a number of instruments. A Keyence laser distance meter was used to measure the bed topography at sub-mm vertical accuracy and 1 mm spatial resolution along the centerline of the flume. The top of the bed ($z = 0$) was defined as the average elevation from this profile, which was 28 mm above the impermeable floor of the flume. That is, the thickness of the subsurface layer was $\eta = 28$ mm (Figure 1). A Massa ultrasonic probe was used to map the water surface topography for each experiment at 50 mm point spacing, and at sub-mm accuracy in the vertical dimension. Local flow depth was calculated as the difference between the water surface elevation and bed elevation, and the average flow depth, h, was calculated as the spatial average along the flume centerline. The local depth was set to zero prior to averaging for points on particles that were partially emerged from the flow. Flow depths ranged from $0.017 < h < 0.52$ m and relative roughness was $0.31 < k_s/h < 9.3$ (Table 1).

Discharge was measured with a Rosemount in-line magnetic flow meter, and depth-averaged flow velocity (U) was calculated following continuity as $U = Q/((h+\eta)W)$ in which $W = 1$ m is the channel width. For a given experiment, we adjusted either the roughness of the inlet ramp into the flume (for $\mathrm{Fr} > 1$) or the tailgate height at the end of the flume (for $\mathrm{Fr} < 1$) to achieve uniform flow across the center 10 m of the flume (i.e., the test section). To verify uniform flow, we calculated a dimensionless flow acceleration factor by averaging along the length of the test section the magnitude of spatial acceleration ($U\frac{dU}{dx} + g\frac{dh}{dx}$) relative to gravitational acceleration due to the sloping bed ($g\sin\theta$), following flow conservation equations for 1-D, steady, depth-averaged flow [*Chow*, 1959]. For all experiments reported here (supporting information Table S1), the dimensionless flow acceleration term was held to less than 20% (and in most cases < 5%). Consequently, we estimate the bed stress assuming steady and uniform flow as $\tau_b = \rho g h \sin\theta$. This method ensures that there are not systematic spatial accelerations across the length of the test section; however, significant temporal and spatial flow accelerations did occur at smaller scales due to turbulence and flow through the roughness layer.

A side-looking Nortek acoustic Doppler velocimeter (ADV) was used to measure a single vertical flow velocity profile located near the center of the test section. Profiles were made for 15 of the 58 experiments (supporting information Table S1) that are representative of nearly the full range of conditions investigated,

except for the steepest slope (30%) where shallow, fast and aerated flows prevented accurate ADV measurements. Owing to the large range of flow conditions and difficulty in making ADV measurements in highly energetic, shallow and bubbly flows, including into the pore spaces between gravel, we did not attempt spatial averaging of velocity profiles, and therefore cannot isolate the form-induced stresses [*Nikora et al.*, 2001; *Manes et al.*, 2007; *Cooper et al.*, 2013]. Nonetheless, the profiles were taken at the exact same location in the flume (with the same fixed cobble bed) for the different experiments, so that profiles can be compared with each other without bias from spatial variations in hydraulics or bed roughness.

For each ADV profile, velocity was measured at ~10 points spaced logarithmically in a transect perpendicular to the average bed surface. For each point, three components of velocity were collected for two minutes at a sampling rate of 200 Hz, and we seeded the water with 44 μm silica to improve signal to noise. Many of the experimental flows were aerated, especially at steep bed slopes, which led to a well-known problem of spike noise [*Goring and Nikora*, 2002]. We used the bivariate kernel density algorithm of *Islam and Zhu* [2013] to despike the ADV data, which was shown to work well in bubbly turbulent jets even when more than 40% of the data are contaminated with spikes. Because the number of points identified as spikes was often a large percentage of the total time series, points were removed from the series rather than interpolated to approximate the affected point. Points were removed in all three directions if they were identified as a spike in one direction. We also removed points using the instrument-reported signal-to-noise ratios less than 15 and correlation coefficients less than 50. Similar to the findings of *Islam and Zhu* [2013], we found that relatively flat spectral density plots prior to filtering, shifted following despiking to near the expected $-5/3$ slope in the inertial subrange for turbulent flow (Figure 4a), giving some confidence to the filtering scheme. Moreover, depth-averaged velocities measured from the ADV profiles match average flow velocities calculated from flow discharge (i.e., $Q/(W(h+\eta))$), which was measured independently from the in-line flow meter (Figure 4b).

Despiked ADV data in the streamwise (u), cross-stream (v) and bed-normal (w) directions were used to calculate the time-averaged local velocities ($\bar{u}$, $\bar{v}$, $\bar{w}$), the standard deviation due to the fluctuating component of velocity (σ_u, σ_v, σ_w), and the streamwise component of the Reynolds stress $-\overline{u'w'} = -\overline{(u-\overline{u})(w-\overline{w})}$, where the overbars denote temporal averages. We also report measurements of the mixing length, following equations (3) and (4) as

$$L = u_*/(d\bar{u}/dz) \tag{20}$$

Turbulence statistics were not computed for time series data with less than 500 points after filtering.

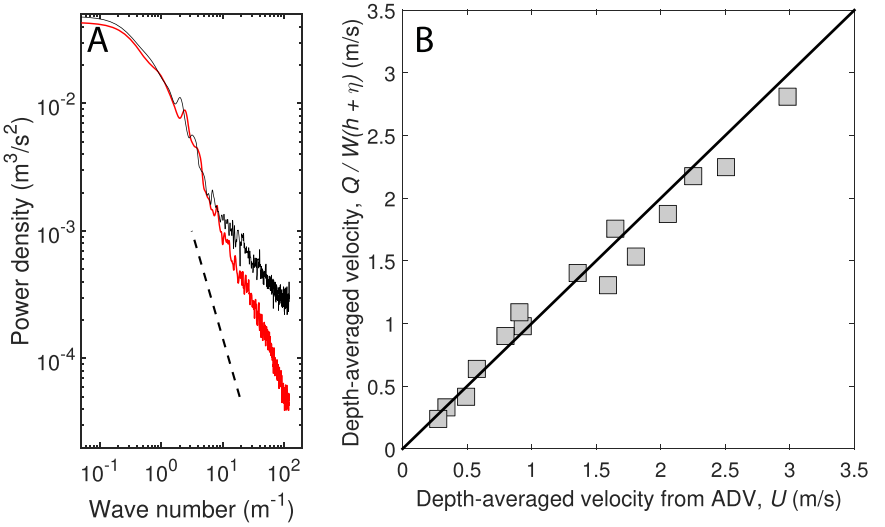

Figure 4. (a) Example power spectral density plot from an ADV measurement during experiments at $z = 2$ mm both before (black) and after (red) filtering for spike noise due to aeration. The dashed line is a $-5/3$ slope which is expected for the inertial subrange in a turbulent flow. The time series was converted to wave number space using the local time-averaged flow velocity following Taylor's frozen turbulence hypothesis. (b) Depth-averaged flow velocities calculated from measurements of total discharge (Q) and flow depth (h) versus those calculated from depth averaging the velocity profile measured from the acoustic Doppler velocimeter (ADV).

Owing to the permeable cobble bed, subsurface ($z < 0$) flow velocities were nonnegligible for some of the experiments. Subsurface flow occurred in a 28 mm thick zone bounded by the impermeable flume floor below and surface flow above. For cases with ADV velocity profiles, the flow velocities at $z = 0$ (i.e., u_0) were calculated by linearly interpolating the vertical velocity profiles, and the depth-averaged surface velocity, U_{surf}, was calculated following equation (17) using finite differences. For the experiments without ADV velocity profiles, the calibrated subsurface flow model (equation (14)) was used to estimate the depth-averaged subsurface velocity, U_{sub}, and then the surface velocity was computed as $U_{surf} = (Q - Q_{sub})/(hW)$, in which $Q_{sub} = U_{sub}\eta W$ is the subsurface discharge.

Mean flow, subsurface flow, and the bulk friction factor are compared with the theory derived in section 3. The roughness length was set to $k_s = 2.5D_{84}$. To apply equation (14) to the exchange layer, we assumed $P = \eta = 28$ mm and found a good fit to our data using $C_1F^* = 1.6$ s^2/m^2 and $K = 1.0$ m/s. These values can be calculated using a fluid kinematic viscosity of $\nu = 10^{-6}$ m^2/s, gravitational acceleration of $g = 9.81$ m/s^2, $C_1 = 2$ and $C_2 = 2$ (corresponding to a linear velocity profile in the exchange layer), porosity in the exchange layer of $\phi_{sub} = 0.5$ (equation (19)), Forchheimer constant of $F = 5 \times 10^{-3}$, and permeability of $k = 10^{-7}$ m^2, in which F and k are slightly larger than values used by *Manes et al.* [2012] for a gravel bed river. The constants are empirical and, for the case of coupled subsurface and surface flow, may differ from those from subsurface flow alone [*Zhou and Mendoza*, 1993]. Turbulence statistics are also given and compared with expectations from *Nezu and Nakagawa* [1993].

5. Results

5.1. General Character of the Flows

The experiments by design crossed a wide range in channel slopes and discharges, and produced flows with depths from 0.03 to 0.52 m and average flow velocities from $U_{surf} = 0.15$ to 3.69 m/s (Table 1). In

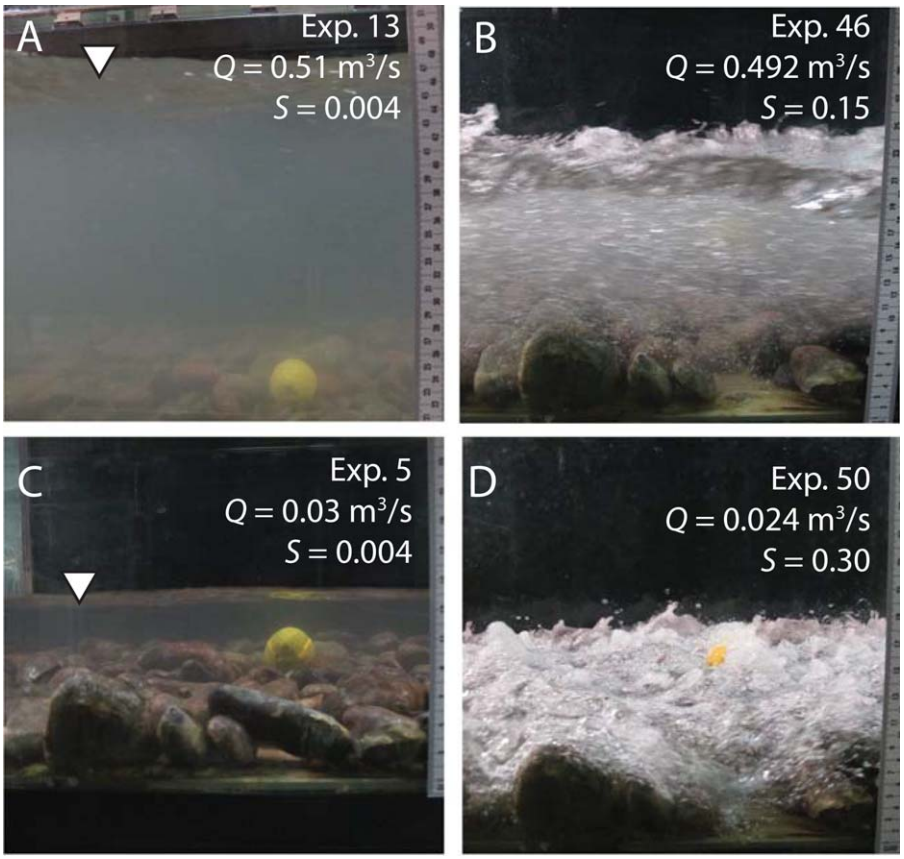

Figure 5. Sideview images of the center of the test section for (a, c) low gradient and (b, d) steep bed slopes, S, and at (c, d) low and (a, b) high discharges, Q. See supporting information Table S1 for corresponding experiment numbers. The yellow cobble is located along the centerline of the flume and has diameters in the downstream and vertical directions of 75 and 74 mm, respectively.

general for the same discharge, flow depths decreased with increasing slope and the flow transitioned from Froude-subcritical to supercritical (Table 1). Increasing channel slope for the same discharge also produced a rougher water surface and more aerated flow (e.g., Figures 5a and 5b). The change in the water surface roughness and aeration was principally a function of channel slope and not flow depth. For example, Figure 5c shows a case where the water surface was smooth despite having a flow depth of the same scale as the bed roughness. In contrast, Figure 5d shows a case with a steep bed slope and shallow flow, in which the flow was aerated as it spilled over the tops of the cobbles. Despite average Froude numbers that were often supercritical, many of the steep and shallow cases visually suggest transcritical flow with shoots and pools occurring at the grain scale (Figure 5d).

5.2. Surface Flow Velocity Profiles

Surface velocity profiles show the expected shape of increasing velocity with distance above the bed (Figure 6a). In general, experiments with steeper slopes and deeper flows had faster flow. Plotted in semilog space, the velocity profiles indicate an increasing deviation from the log law (equation (2)) with distance toward the bed (Figure 6b). Near-bed velocities also were significantly larger than predicted by the hybrid mixing-length model without inclusion of subsurface velocities (equation (11)), which is especially true for experiments with steep bed slopes in which subsurface velocities were large. As shown in Figure 6c, despite the wide range in channel slopes and relative roughness values, all of the velocity profiles collapse to the prediction given by equation (10), which accounts for both grain-scale turbulent mixing and subsurface velocities. Grain-scale mixing accounts for the deviation from a logarithmic profile (i.e., profile curvature near the bed in log linear space), and subsurface flow accounts for the offset of some profiles to higher velocities near the bed. Both the observations and our new theoretical model converge to the log law far above the bed.

Mixing lengths for the experimental data are scattered but in general indicate larger mixing lengths with distance away from the bed—consistent with Prandtl's hypothesis (equation (5))—for $z/k_s > 0.1$, and a more uniform mixing length closer to the bed consistent with equation (6) (Figure 7). The hybrid mixing-length model (equation (7)) captures this transition across the roughness layer to the logarithmic layer. The hybrid

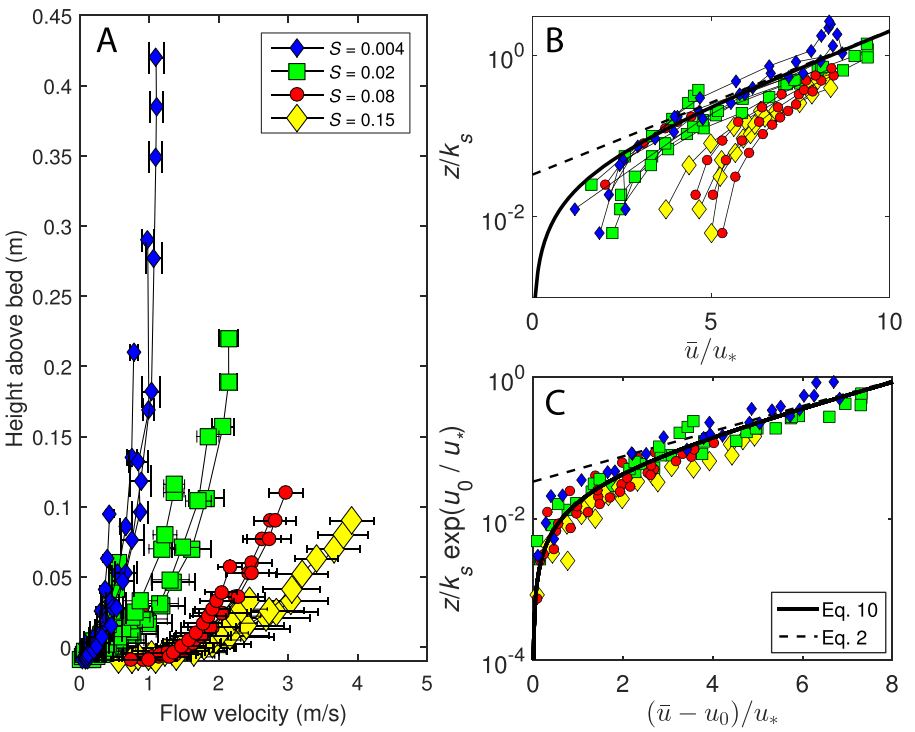

Figure 6. (a) Velocity profiles for all 15 experiments with ADV profiles (see supporting information Table S1). (b, c) Dimensionless velocity profiles compared with the log law (equation (2)), assuming $u_0 = 0$, and the hybrid mixing-length model (equations (10) and (11)) assuming (Figure 6a) no subsurface flow and (Figure 6b) accounting for the observed subsurface flow.

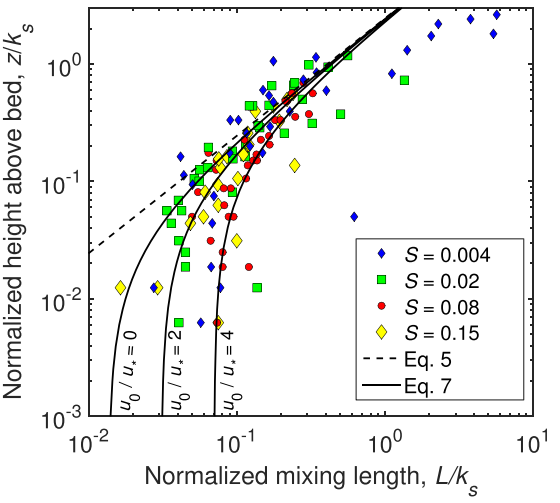

Figure 7. Turbulent mixing length (L) as a function of height above the bed as calculated from the velocity data for all the experiments with ADV profiles using (equation (20)), and predictions using Prandtl's mixing-length model (equation (5)) and the hybrid mixing-length model (equation (7)). All length scales are normalized by the bed roughness height, k_s.

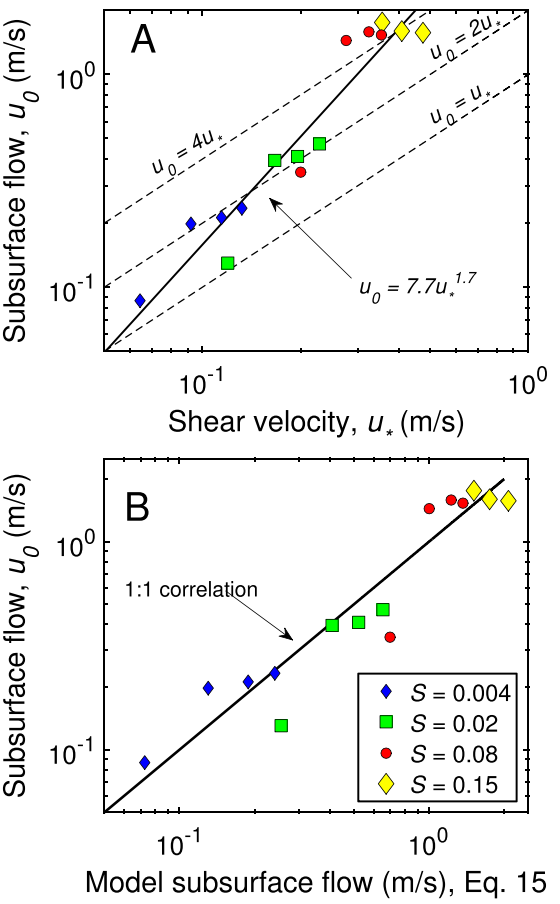

Figure 8. Time-averaged flow velocities at the bed surface, $u_0 = \bar{u}(z=0)$, plotted versus (a) the bed shear velocity and (b) predictions from the modified Darcy-Brinkman-Forchheimer equation (equations (14) and (15)).

mixing-length model also provides an explanation for some of the scatter in the observations as a result of differing subsurface flow velocities (Figure 7), which emerges in the model because mixing in the roughness layer is a function of subsurface flow velocity relative to the shear velocity (equation (9)).

5.3. Subsurface Flow

Subsurface flow velocities at $z = 0$ ranged from $u_0 = 0.16$ to 2.26 m/s, with inferred depth-averaged subsurface flow velocities in the exchange layer of $U_{sub} = 0.04$–0.57 m/s (Figure 8a). All subsurface flows were turbulent with Reynolds numbers, $\mathrm{Re}_{sub} = U_{sub}D_{50}/\nu$, ranging from 8×10^2 to 4×10^4 (supporting information Table S1). Based on previous work for turbulent shear flow over a vegetated canopy with negligible bed slope, we might expect u_0 to scale linearly with u_* (i.e., equation (16)) with a coefficient of order unity [*Ghisalberti*, 2009]. Figure 8 shows that most data are bounded by $2 < u_0/u_* < 4$; however, the best fit line in a least squares sense, $u_0 = 7.7u_*^{1.7}$, is nonlinear with larger values of u_0/u_* corresponding to steeper channel-bed slopes. We expect that the nonlinear dependence of u_0 on u_* in our experiments is because subsurface flow is driven by both shear from the overlying surface flow (as in the vegetated canopy studies) and by gravity acting on the subsurface water itself owing to the steep bed slopes. The subsurface model that considers both of these effects (equations (14) and (15)) predicts higher ratios of u_0/u_* on steeper slopes, and better matches the observations than the linear model (Figure 8b).

5.4. Turbulence

Figure 9 shows the three components of velocity fluctuations, as well as the streamwise Reynolds stress. As expected from previous work in lower sloping and deeper flows, the velocity fluctuations generally increase toward the bed, peak near the top of the cobbles, and decrease deeper into the cobble bed [*Nezu and Nakagawa*, 1993; *Nikora and Goring*, 2000].

The normalized Reynolds stresses ($-\overline{u'w'}/u_*^2$; Figure 10a) are less than their expected value of unity near the bed [*Nezu and Rodi*, 1986], which is likely due to strong spatial variations in the flow structure and form-induced stresses within the roughness layer that are not captured by our single profile [*Nikora et al.*, 2001; *Coleman et al.*, 2007; *Cooper et al.*, 2013]. The near-bed Reynolds

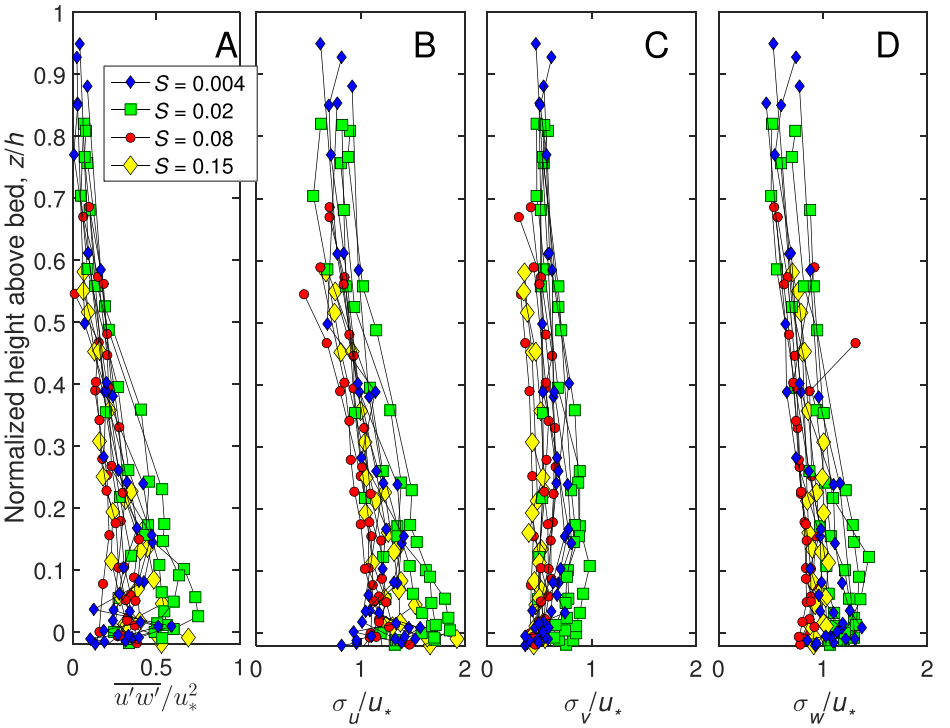

Figure 9. Profiles of (a) normalized Reynolds stresses, and turbulence intensities in the (b) downstream (σ_u), (c) cross-stream (σ_v), and (d) bed-normal (σ_w) directions as a function of normalized height above the bed. Data are for all 15 experiments with ADV profiles (supporting information Table S1).

stresses show no clear differences between experiments with different channel slopes (Figure 12a). The data suggest that peak Reynolds stresses might be highest when $h \sim k_s$; however, it is unclear if this trend is robust.

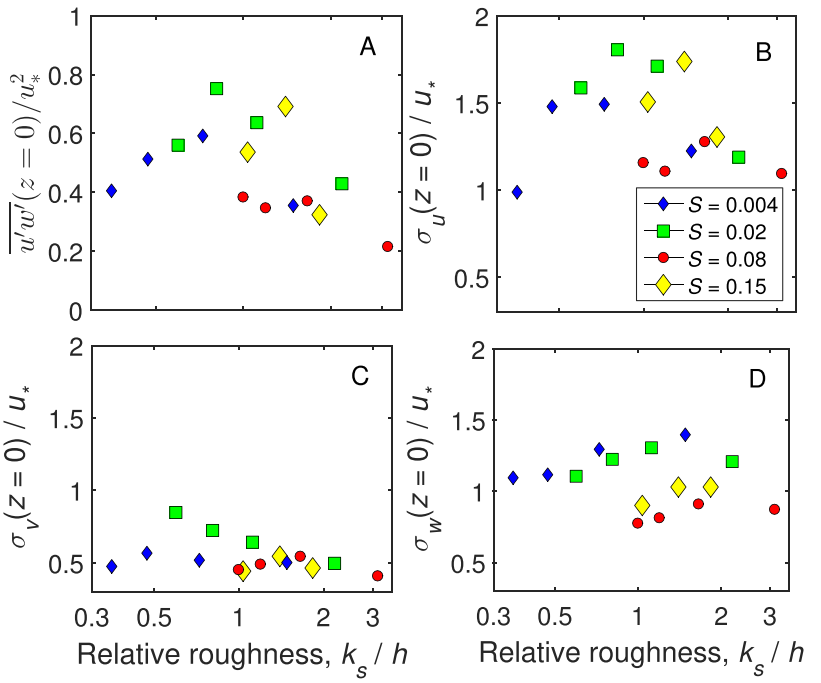

Figure 10. Near-bed values (linearly interpolated at $z = 0$) of (a) normalized Reynolds stresses, and turbulence intensities in the (b) downstream (σ_u), (c) cross-stream (σ_v), and (d) bed-normal (σ_w) directions as a function of relative roughness.

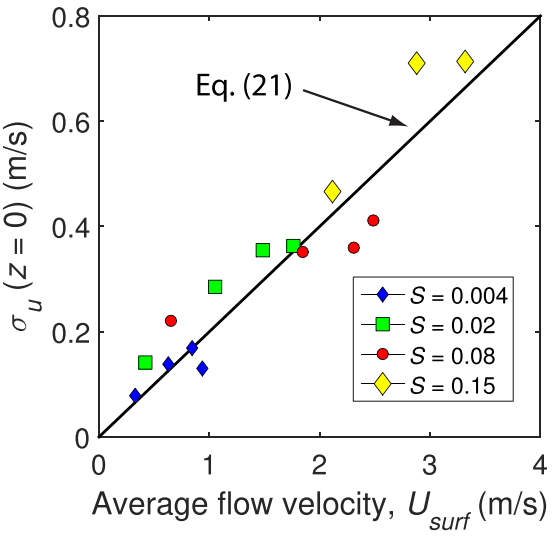

Figure 11. Near-bed values (linearly interpolated at $z = 0$) of turbulence intensities in the downstream (σ_u) direction as a function of depth-averaged surface flow velocity. The solid line is the linear relation given by $\sigma_u = 0.2U_{surf}$ (equation (21)) as proposed by *Lamb et al.* [2008].

Peak near-bed fluctuations in the streamwise direction are $\sigma_u/u_* \sim 1.5$ (Figure 10b), which is smaller than typically found in flows with lower relative roughness [*Nezu and Rodi*, 1986], and consistent with the idea that near-bed streamwise velocity fluctuations are smaller in rough and shallow flows [e.g., *Lamb et al.*, 2008]. Cross-stream near-bed velocity fluctuations are $\sigma_v/u_* \sim 0.5$, similar to expectations from deeper flows [*Nezu and Rodi*, 1986], and show no strong variations with channel slope or relative roughness (Figure 10c). Bed-normal (i.e., near vertical) near-bed velocity fluctuations are $\sigma_w/u_* \sim 1$, which is also similar to expectations for deeper flows (Figure 10d). However, σ_w/u_* decreases with increasing channel slope (Figure 10d), which may be due to the spilling flow over the cobble bed in those experiments.

Lamb et al. [2008] proposed that near-bed streamwise velocity fluctuations in rough mountain streams scale better with the depth-averaged flow velocity, as compared with u_*, owing to depth-scale turbulent structures. Their compilation of previous work indicated

$$\sigma_u = a_1 U_{surf} \tag{21}$$

with $a_1 \sim 0.2$. Equation (21) can explain much of the variance in our experimental data for σ_u across the entire range in channel slope and relative roughness ($r^2 = 0.83$) (Figure 11). However, we found no improvement in characterizing σ_v or σ_w with U as compared with u_*.

5.5. Depth-Averaged Flow and Friction Factor

Observed bulk friction coefficients, $C_{f,surf}$ and $C_{f,total}$, for deep flows ($k_s/h < \sim 0.3$) are small ($\sim 10^{-2}$) and increase with increasing relative roughness following previous theory for planar beds (i.e., equation (1)) (Figure 12). However, the bulk friction coefficients for shallow flows increase substantially as the flow shallows ($k_s/h > 1$) with C_f values that exceed unity for $k_s/h > 5$. The trend in C_f versus relative roughness appears to be robust regardless of the channel slope or Froude number. For these shallow flows, our observations deviate substantially from equation (1)—a commonly used baseline grain resistance formula. For example, equation (1) underpredicts the observed $C_{f,surf}$ and $C_{f,total}$ for $k_s/h = 5$ by a factor of ~50, whereas the hybrid mixing model (equation (19)) is in better agreement with the observations. The observed bulk friction coefficients are also similar to the relation of *Ferguson* [2007], which is a good representation of the average flow resistance in natural streams [*Rickenmann and Recking*, 2011], with our measurements of $C_{f,total}$ within a factor of 0.26 (median) of the Ferguson relation.

The model and most of the observations indicate that $C_{f,total}$ is larger than $C_{f,surf}$, indicating slower flow and greater flow resistance in the subsurface flow layer as compared to the surface flow. However, the difference is relatively minor. For cases of low relative roughness and low bed slopes, flow resistance in the subsurface layer is high, but the subsurface discharge is negligible compared to the total discharge (Table 1), such that $C_{f,total} \approx C_{f,surf}$ (Figure 12). The discharge in the subsurface layer is not negligible for cases with steep slopes and high relative roughness; however, for these cases the subsurface flow velocities are larger and flow resistance in the subsurface is similar to the surface layer, and thus again $C_{f,total} \approx C_{f,surf}$. The greatest difference between $C_{f,total}$ and $C_{f,surf}$ occurs for cases with both low relative roughness and low bed slopes because, for these cases, the subsurface velocity is small compared and the subsurface layer thickness is large relative to the surface flow.

The open symbols in Figure 12a show the friction coefficient under the common assumption that the subsurface discharge is negligible (i.e., $U_{surf} \approx Q/hW$), as a comparison to the filled symbols where

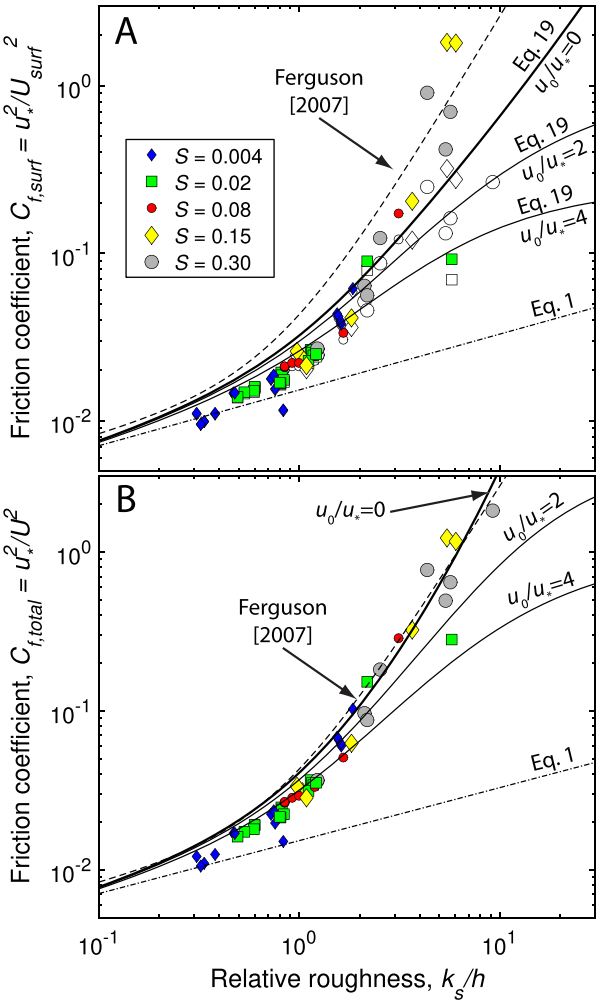

Figure 12. Bulk friction coefficient for (a) the surface flow alone ($C_{f,surf}$) and (b) for the surface and subsurface flow combined ($C_{f,total}$) as a function of relative roughness for all 58 experiments (supporting information Table S1). The data are compared to equation (1) that is designed for planar, gravel bed rivers (i.e., no macro-scale form drag) and often taken to be a "base case" for flow resistance partitioning attributed to grain drag; *Ferguson* [2007] (using their recommended values of $a_1 = 6.5$ and $a_2 = 2.5$) that matches well observations in steep mountain streams that contain macro-scale form drag; and our hybrid mixing-length model (solid lines) for different specified values of subsurface flow. In Figure 12a, the filled symbols represent the values of $C_{f,surf}$ accounting for the subsurface flow in the calculation of the surface flow, that is $U_{surf} = (Q - Q_{sub})/hW$. The open symbols are the values of $C_{f,surf}$ under the common assumption of negligible subsurface flow, that is $U_{surf} = Q/hW$.

$U_{surf} = (Q - Q_{sub})/hW$. Despite the thickness of the subsurface layer being only $\eta = 28$ mm (or $\sim 0.5D_{50}$), neglecting the subsurface discharge results in an erroneous reduction $C_{f,surf}$ by as much as an order of magnitude for cases with steep slopes and high relative roughness (Figure 12a).

6. Discussion

6.1. Vertical Velocity Profile

The hybrid mixing-length approach allows a simple derivation of the vertical velocity profile across the roughness layer and the rest of the surface flow. It matches our observations better than the approach proposed by *Lamb et al.* [2008] of matching solutions between the two layers with independent mixing lengths for each layer. A similar velocity profile using a hybrid mixing length [*Christensen*, 1972] also was found to characterize well the velocity profile from the steep flume experiments of *Mizuyama* [1977]. Importantly, the hybrid approach does not produce a discontinuity in velocity or stress at the top of the roughness layer and allows the velocity profiles to deviate from logarithmic within the roughness layer. Our mixing-length estimates also support the hybrid mixing-length hypothesis because they vary smoothly over the roughness layer from constant near $z = 0$ to near linear at $z \gg k_s$ (Figure 7). We expect the model to be applicable to other rivers as long as beds are planar and bed roughness Reynolds numbers are in the fully turbulent regime.

Experiments on flow over vegetation indicate that there is commonly an inflection point in the vertical velocity profiles in the subsurface [*Katul et al.*, 2002; *Nepf*, 2012], which we do not observe in our experiments, nor was it observed in other steep stream experiments with planar beds [*Mizuyama*, 1977]. One reason for this difference may be that our subsurface layer is thin, and that a thicker bed may be needed to produce an inflection point deeper in the subsurface. In addition, experiments designed to simulate vegetation stems often use vertical cylinders that creates a step-like discontinuity in porosity and permeability, whereas the transition from surface to subsurface flow across the roughness layer for a gravel bed is more gradual (e.g., equation (18)) [*Nikora et al.*, 2001]. Subsurface flow velocities for the steep sloping cases in our experiments also were much larger than in most experiments with flow over vegetation, and this high velocity subsurface flow may prevent the development of an inflection point on steep slopes.

There is a drastic change in the appearance of the flows from placid with a smooth water surface at low slopes and subcritical Froude numbers, to spilling and aerated flow at very steep slopes and supercritical

Froude numbers (Figure 5). It is surprising, however, that the mean flow velocity profiles collapse to the same relationship regardless of channel slope and Froude number, as long as shear velocity and subsurface flow are taken into account (Figure 6c). In fact, equation (11) indicates that there is no effect of channel slope, Froude number or relative roughness on mean flow velocity profiles (i.e., on $\overline{u}(z)/u_*$) for the case of negligible subsurface flow. While we do find that flow velocities within the roughness layer deviate substantially from logarithmic, the flow profiles in the roughness layer are self-similar whether the flow is deep or shallow. This is not what we expected given the visual change in the character of the flow (Figure 5) and previous ideas that shallow flow over roughness significantly affects the flow profile [*Lawrence*, 1997; *Aberle and Smart*, 2003; *Wilcox et al*., 2006; *Ferguson*, 2007]. For example, our findings are counter to the models of *Lamb et al*. [2008] and *Recking* [2009], which both proposed reduced mean flow velocities within the roughness layer for shallow flows with high relative roughness. Our results instead show that local time-averaged flow velocities within the roughness layer (equation (11)) are insensitive to relative roughness (k_s/h), except through its influence on subsurface velocity.

6.2. Importance of Subsurface Flow

Our experiments produced a wide range of subsurface flow velocities, which were small for low bed slopes and large for steep bed slopes. The finding of $u_0 \propto u_*^{1.7}$ is unlikely to be universal and instead reflects the flow depth and slope combinations that were possible in the flume experiments. Equation (14), on the other hand, should hold for any combination of slope and u_* and allows the model to be adapted to different grain sizes and grain-size distributions through input values of porosity and permeability. For the steep sloping experiments, the subsurface flow affects not only the flow velocities at the bed surface but also the apparent mixing length, structure of the mean velocity throughout the flow depth, and the bulk friction factor. Unlike most studies of flow through vegetation where subsurface flow velocities are driven by shear from the overriding surface flow [*Nepf*, 2012], our experiments indicate that on steeper slopes, subsurface flow is also driven by gravity acting directly on the subsurface fluid (i.e., there is a hydraulic head gradient), which results in higher subsurface flow velocities than predicted from surface flow shear alone. While enhanced mixing between the surface and subsurface flows may cause higher friction factors for low sloping channels with negligible subsurface flow velocity [*Manes et al*., 2011b; *Cheng et al*., 2016], our model and measurements of the velocity profile show that faster subsurface flow velocities on steep slopes result in faster surface flows, and hence overall lower friction factors (Figure 12).

It is surprising that subsurface flow had such an impact on the surface flow in our experiments because the alluvial bed was only about one grain-diameter thick, with the subsurface layer only 28 mm thick, or about one-half of D_{50}. In addition, for the experiments with ADV profiles, the measured subsurface discharge was typically only a few percent of the total discharge, and less than 6% of the total discharge for all cases—a fraction similar to what was found by *Recking et al*. [2008b] in flume experiments with $S < 10\%$. In our steepest ($S = 0.3$) and shallowest cases without ADV profiles, subsurface discharge was as much as half of the total discharge (Table 1). Thus, in addition to explaining changes in the surface velocity profile for steep bed slopes, subsurface discharge might also explain why some previous workers report lower frictional resistance for planar, coarse-grained beds than reported here. For example, as illustrated in Figure 12a, if subsurface discharge is assumed negligible, which is often the case in flume experiments where only the total discharge is measured [*Mizuyama*, 1977; *Bathurst et al*., 1981], then the surface velocity will be overestimated, resulting in a lower estimate of flow resistance. In our experiments, this error would bias the frictional resistance low by as much as a factor of ten for the steep, shallow cases (Figure 12a).

Our flume experiments motivate the need for more work on subsurface flow through alluvial beds in steep mountain streams. The experiments used a relatively narrow grain-size distribution ($D_{84}/D_{50} = 1.3$) and a wider distribution, more typical of gravel bed rivers (e.g., $D_{84}/D_{50} = 3$) might reduce subsurface velocities. For example, filling of pore spaces with fines could reduce subsurface velocities, and this could be accounted for in equation (14) by modifying the porosity and permeability. However, natural channels at $S > 0.1$ tend to have boulder beds that are much coarser than in our experiments, which could increase permeability and make subsurface flow more important than in our experiments. In addition, the thickness of the subsurface layer in our experiments was only $\sim 0.5D_{50}$; thicker beds of permeable alluvium are expected for natural streams, which may make subsurface flow more important in those cases. Beyond flow hydraulics, high rates of subsurface flow may influence nutrient cycling [*Packman et al*., 2004], capture and

transport of fines and organic carbon [*Wang et al.*, 2015], and lead to destabilization of the bed at steep slopes producing debris flows [*Kean et al.*, 2013; *Prancevic et al.*, 2014].

6.3. Flow Resistance and Stress Partitioning

One of the main motivations to conduct these experiments was to determine the bulk friction coefficient for the purpose of stress partitioning [*Einstein and Barbarossa*, 1952]. In terms of friction factors, linear stress partitioning indicates that the total frictional resistance, C_{fT}, is given by the sum of the friction factor due to grain drag, C_{fg}, and morphologic form drag, C_{fm},

$$C_{fT} = C_{fg} + C_{fm} \tag{22}$$

Stress partitioning is typically thought to be necessary to make accurate predictions of sediment transport because only grain drag acts to move sediment, and morphologic form drag might dominate the momentum budget [*Millar*, 1999; *Rickenmann*, 2001; *Aberle and Smart*, 2003; *Wilcox et al.*, 2006; *Yager et al.*, 2007; *Nitsche et al.*, 2011]. A common approach to determine the morphologic form drag is to subtract the grain drag from the measured or estimated total stress [*Einstein and Barbarossa*, 1952]. Grain drag in turn is commonly calculated from well-known empirical relations like equation (1) developed in large part from flume experiments over low sloping planar beds.

Our flume experiments lacked bed forms and channel forms (i.e., $C_{fm} = 0$) such that the total friction factor we measured (Figure 12) is equivalent to that due to grain drag alone, C_{fg}. Our results show that C_{fg} for planar beds with high relative roughness and large particle Reynolds numbers deviate significantly from relations developed for lower gradient rivers, similar to some previous findings for steep, planar-bedded streams [*Mizuyama*, 1977; *Bathurst et al.*, 1981; *Cao*, 1985; *Bathurst*, 2002; *Recking et al.*, 2008a; *Prancevic and Lamb*, 2015b]. The hybrid mixing-length model and measurements of the velocity profile indicate that the high flow resistance in shallow, rough flows can be explained as a result of (1) a grain-scale mixing length in the roughness layer and (2) a roughness layer that comprises an increasing fraction of the total flow depth for shallow, rough flows. Thus, baseline C_{fg} values are much larger in mountain streams as compared with deeper rivers, even in the absence of morphologic form drag from bed forms and channel forms and immobile boulders. In fact, our flume data align with typical measured values of C_{fT} from natural mountain streams (that have bed forms and channel forms and immobile boulders), which are represented in Figure 12 by the empirical model of *Ferguson* [2007] that has been shown to be a good predictor of average flow resistance in natural rivers [*Rickenmann and Recking*, 2011]. The implication is that morphologic form drag may play a smaller role in mountain streams than commonly assumed. For example, following the approach recommended by *Rickenmann and Recking* [2011] and *Ferguson* [2012] to calculate C_{fT} from *Ferguson* [2012] and C_{fg} from equation (1), one might conclude that morphologic form drag accounts for an increasingly large fraction of the momentum budget for shallow, rough flows, reaching 95% or more for $k_s/h > 3$. In contrast, measured grain drag from our experiments compare well with the field-calibrated model of *Ferguson* [2007], suggesting that morphologic form drag does not change significantly with relative roughness and is only 20–30% of the total flow resistance.

The flume experiments are simple representations of steep mountain streams, but this is unlikely to be the cause of heightened flow resistance in the experiments. For example, bed load transport, which was purposefully excluded in our experiments, tends to increase flow resistance for planar beds [*Wiberg and Rubin*, 1989; *Recking et al.*, 2008a]. If the subsurface layer was filled with fines, subsurface flow would be reduced, which would lead to slower surface flow (equation (10)) and hence even greater flow resistance. A wider grain-size distribution on the bed would also result in enhanced flow resistance because the coarse fraction tends to dominate flow resistance. Wall roughness and channel curvature would also cause larger flow resistance. Thus, we expect these complicated scenarios common to natural channels to have higher flow resistance than our experiments, even for planar beds, which would reduce further the inferred role of morphologic form drag.

Our results are consistent with *Zimmermann* [2010] who found that experiments with planar, rough beds had nearly identical flow resistance as similar experiments with step-pool bed forms. They had expected the experiments with step pools to have higher flow resistance due to morphologic form drag; but this was not observed. Others also have noted an increase in the flow resistance from grain drag for shallow, rough flows [*Bathurst*, 1985; *Lawrence*, 2000; *Bathurst*, 2002; *Carling et al.*, 2002] and often this is attributed to

increased energy losses from highly 3-D flow, flow spilling over grains, transcritical flow, and standing waves in shallow flow. It is important to note, however, that we find that the vertical structure of flow velocity within the roughness layer to be similar for deep flows as for shallow flows (Figure 6c). Thus, energy losses associated with free surface effects for shallow flow, such as spilling flow, transcritical flow, and standing waves, also need not be invoked to explain the observed friction factors. All that is needed to explain the flow resistance data in our experiments is that the roughness layer becomes an increasing fraction of the total flow depth for shallow flows.

6.4. Implications for Sediment Transport

If grain drag dominates flow resistance in steep channels, why then do sediment transport relations calibrated for deep flows fail in steep channels with high relative roughness? *Schneider et al*. [2015b] showed that bed load transport observations in mountain streams can be empirically fit equally well using either a stress-partitioning scheme based on a baseline relation like equation (1), or through use of a heightened critical Shields number for incipient sediment motion, τ_{*c}. Given uncertainty in the stress-partitioning concept applied to steep mountain streams, here we focus on reasons for a heightened critical Shields number. *Prancevic et al*. [2014] and *Prancevic and Lamb* [2015b] found that the heightened Shields numbers observed in natural steep streams can be reproduced in experiments with planar beds of near uniform gravel that lacked morphologic form drag from bed forms and channel forms and large immobile grains. Thus, like heightened flow resistance, heightened τ_{*c} in steep streams with high relative roughness appears to require an explanation that is independent of macro-scale morphologic form drag [*Lamb et al*., 2008].

Forces on bed sediment at initial motion can be conceptualized as the product of the square of near-bed velocity and a drag or lift coefficient [*Wiberg and Smith*, 1987b]. Using stress-partitioning ideas, several models have attempted to explain heightened critical Shields numbers by assuming that near-bed velocities decrease with large relative roughness [*Lamb et al*., 2008; *Recking*, 2009; *Ferguson*, 2012]. However, our results show that local time-averaged velocity within the roughness layer is insensitive to relative roughness, and therefore changes in the structure of the mean flow are unlikely to be the reason behind higher critical Shields stresses at initial motion in shallow, rough flows. By process of elimination, this points to increased bed stability due to grain structuring, changes in drag and lift coefficients, or changes in the structure of turbulence which impacts peak hydrodynamic forces acting on particles.

Bed structuring may play a role in reducing transport rates, especially where boulders form steps and particle clusters [*Church et al*., 1998; *Zimmermann et al*., 2010], but evidence is lacking to support bed structuring being the dominant reason for heightened critical Shields numbers in steep rivers. Using a force meter, *Prancevic and Lamb* [2015a] found the friction angle in natural streams for boulders organized in steps to be greater than those not in steps, but no systematic differences in grain friction angles as a function of channel slope. In addition, the experiments of *Prancevic et al*. [2014] and *Prancevic and Lamb* [2015b], which found higher critical Shields numbers with steeper slopes (and higher relative roughness), lacked systematic changes in bed structuring with slope. These findings then point to drag and lift coefficients and turbulence as the mechanisms behind lower than expected sediment transport rates in steep channels.

To our knowledge, drag and lift coefficients have not been measured systematically in steep streams across a wide range of channel-bed slopes with coarse beds and shallow flow depths, and consequently they are often assumed to be independent of relative roughness and channel slope [*Lamb et al*., 2008; *Recking*, 2009]. For an isolated hemisphere on a smooth bed, *Flammer et al*. [1970] showed that drag forces increase with greater relative roughness due to a number of effects, including surface waves, especially for subcritical flows. Similar trends of increasing C_D due to wave drag were inferred from studies of block entrainment [*Lawrence*, 2000; *Carling et al*., 2002] and from forces on bridge piers [*Hay*, 1947; *Chaplin and Teigen*, 2003]. Thus, if anything, it appears that C_D increases with relative roughness, which should make sediment transport more efficient in steep channels, opposite of what is observed. It seems likely that lift decreases as the flow shallows and slows over the tops of grains [*Carling et al*., 2002; *Lamb et al*., 2008], which would make sediment more stable on steeper slopes. However, direct measurements of lift under conditions of high relative roughness have not been made.

In support of the hypothesis of *Lamb et al*. [2008], we find evidence that part of the cause of heightened critical Shields numbers in steep streams is from reduced intensity of turbulence for streams with high relative roughness [*Wang et al*., 1993; *Dittrich and Koll*, 1997; *Carollo et al*., 2005]. *Lamb et al*. [2008] explained

the dependence of near-bed turbulence on relative roughness as a result of depth-scale eddies with velocities that correlate with the depth-averaged flow rather than the local flow [see also *Nowell and Church*, 1979; *Recking et al*., 2008a]. Our turbulence measurements (Figure 11) support the data compilation of *Lamb et al*. [2008] that downstream-directed velocity fluctuations scale better with the depth-averaged flow velocity than the bed shear velocity, resulting in reduced magnitude of velocity fluctuations for flows with high relative roughness. *Lamb et al*. [2008] showed theoretically that the reduction in the magnitude of turbulent fluctuations can account for a significant fraction of the observed increase in the critical Shields number at incipient motion with increasing channel slope. Because the near-bed turbulent fluctuations (σ_u) scale linearly with the depth-averaged flow velocity (Figure 11), the square of turbulence intensity (σ_u/u_*) must then be inversely proportional to the bulk friction coefficient (C_f). That is,

$$\left(\frac{\sigma_u}{u_*}\right)^2 \propto \left(\frac{U}{u_*}\right)^2 \equiv \frac{1}{C_f} \tag{23}$$

Equation (23) may help explain why stress-partitioning approaches have had success in explaining initial sediment motion and sediment flux data on steep slopes [*Rickenmann*, 2001; *Nitsche et al*., 2011; *Ferguson*, 2012; *Yager et al*., 2012], even if flow resistance is largely dominated by grain drag. Sediment transport is affected by near-bed turbulence, and our results show that it is near-bed turbulence, rather than the mean flow in the roughness layer, that depends on flow resistance through the scaling between near-bed turbulence and the depth-averaged flow velocity. For example, the critical Shields number has been argued to scale as [*Lamb et al*., 2008]

$$\tau_{*c} \propto \left(\frac{u_*}{\langle\overline{u}\rangle + \sigma_u}\right)^2 \tag{24}$$

in which $\langle\overline{u}\rangle$ is the time-averaged velocity integrated spatially across a grain. Combination of equations (21), (23), and (24) with $\alpha_1 = 0.2$ (Figure 11) and $\langle\overline{u}\rangle = \alpha_2 u_*$, where α_2 is an order one constant that depends on the subsurface velocity (Figure 6b), yields a near-power law relation between the critical Shields number and C_f

$$\tau_{*c} \propto C_f^{\gamma} \tag{25}$$

in which γ is about one third. For example, γ ranges from 0.32 to 0.14 for $1 < \alpha_2 < 3$. Thus, the near-bed turbulence hypothesis of *Lamb et al*. [2008] for heightened τ_{*c} implies a power law relation between τ_{*c} and C_f with a power of about $\gamma = 1/3$ for cases with negligible subsurface velocity. These ideas are well supported by the experiments of *Prancevic and Lamb* [2015b] who found a strong power law relation between τ_{*c} and C_f with the best fit γ of 0.34.

In summary, our analysis suggests that while flow resistance and sediment transport depend on relative roughness, they might not be causally linked as implied in stress-partitioning models. Instead, flow resistance increases with relative roughness because the roughness layer occupies a larger portion of the total flow depth for shallow flows. The local time-averaged flow velocities within the roughness layer, however, are insensitive to changes in relative roughness. In contrast, the intensity of near-bed turbulence is reduced in shallow, rough flows (following linear scaling with the depth-averaged flow velocity) which results in an increase in critical Shields number and a decrease in sediment flux with large relative roughness, and a power law relation between τ_{*c} and C_f. At conditions of initial motion, high relative roughness necessarily correlates with steeper bed slopes [*Prancevic and Lamb*, 2015b], thus producing a correlation between high τ_{*c}, large C_f, reduced sediment flux, and steep bed slopes in mountain streams.

7. Conclusions

We present a new 1-D theory for the vertical structure of mean flow velocity and the associated bulk friction factor and compare the theory to a series of flume experiments made with a planar bed of fixed natural cobbles over a wide range of bed slopes (0.004–0.3) and relative roughness values (0.31–9.3) common to mountain streams. We find that flow velocity in steep, rough flows has a nearly logarithmic vertical velocity profile far above the bed; however, flow velocity decreases less than logarithmically as the bed is approached, and is nonzero at the average-bed elevation ($z = 0$). These velocity profiles match a new theory

for flow above and within a high-Reynolds-number roughness layer derived using a hybrid eddy viscosity model. The measured velocity profiles are self-similar and are a function of bed shear stress, bed roughness and the subsurface flow velocity with no independent dependencies on flow depth, relative roughness, channel slope or Froude number. Thus, the local time-averaged flow velocity in steep, rough streams with planar beds is remarkably similar to that in lower gradient gravel bed rivers despite obvious visual differences in the water surface including rough, spilling and aerated flow in the steep cases.

Our experiments produced significant subsurface flow through the cobble bed at steep slopes, which created a nonzero "slip velocity" at the bed surface. The slip velocity at the bed surface affected the magnitude and shape of the velocity profile within the roughness layer and higher into the surface flow. We found agreement between subsurface flow velocities and a modified Darcy-Forchheimer-Brinkman equation that accounts for both the bed slope and shear from the overriding surface flow to drive subsurface flow.

Regardless of channel slope and Froude number, we find that flow resistance increases significantly with increasing relative roughness, and closely matches observations from natural mountain streams. The close comparison between natural mountain streams and our experiments is surprising because the experiments lacked bed forms, immobile boulders or other sources of macro-scale form drag that are thought to dominate flow resistance in natural channels. The flow resistance observations can be explained as a result of high grain drag in the roughness layer, and the fact that the roughness layer occupies an increasing portion of the total flow depth in shallow flows. These results call into question the applicability of stress-partitioning techniques in mountain streams, and suggest that macro-scale form drag in mountain streams may be significantly less than typically assumed.

Near-bed velocity fluctuations were in general lower than expected for cases with deep flows and smooth beds, and the strongest correlation was between streamwise turbulence intensity and the depth-averaged flow velocity, rather than bed shear velocity. Thus, while local time-averaged flow velocity appears to be independent of flow depth and relative roughness, near-bed turbulence intensities are a function of relative roughness through scaling with the depth-averaged flow velocity. These results support the idea that reduced sediment transport rates in steep streams may be due to reduced turbulence intensities that occur in flows with high relative roughness, rather than changes to the local-mean flow. Thus, while steep steams tend to have both high flow resistance and reduced sediment transport rates, the two may not be causally linked through macro-scale form drag as implied in stress-partitioning techniques, but instead covary with relative roughness for different reasons.

Acknowledgments

Funding for this work was provided by the National Science Foundation EAR-0922199 and EAR-1349115, and the Caltech Terrestrial Hazard Observation and Reporting program. This work benefited from helpful discussions with Rob Ferguson, Jeff Prancevic, and Heidi Nepf, and formal reviews by Dieter Rickenmann and other reviewers. Data from the experiments are provided in the supporting information Table S1 or by e-mail request to M. Lamb.

References

Aberle, J., and G. M. Smart (2003), The influence of roughness structure on flow resistance on steep slopes, *J. Hydraul. Res.*, *41*(3), 259–269.

Bathurst, J. C. (1985), Flow resistance estimation in mountain rivers, *J. Hydraul. Eng.*, *111*(4), 625–643.

Bathurst, J. C. (2002), At-a-site variation and minimum flow resistance for mountain rivers, *J. Hydrol.*, *269*(1–2), 11–26, doi:10.1016/S0022-1694(02)00191-9.

Bathurst, J. C., R. M. Li, and D. B. Simons (1981), Resistance equation for large-scale roughness, *J. Hydraul. Div. Am. Soc. Civ. Eng.*, *107*(12), 1593–1613.

Bathurst, J. C., W. H. Graf, and H. H. Cao (1987), Bed load discharge equations for steep mountain rivers, in *Sediment Transport in Gravel-Bed Rivers*, edited by C. R. Thorne, J. C. Bathurst, and R. D. Hey, pp. 453–477, John Wiley, Chichester, U. K.

Battiato, I. (2012), Self-similarity in coupled Brinkman/Navier-Stokes flows, *J. Fluid Mech.*, *699*, 94–114, doi:10.1017/jfm.2012.85.

Bear, J. (1972), *Dynamics of Fluids in Porous Media*, p. 764, Elsevier, New York.

Beavers, G. S., and D. D. Joseph (1967), Boundary conditions at a naturally permeable wall, *J. Fluid Mech.*, *30*, 197–207, doi:10.1017/S0022112067001375.

Buffington, J. M., and D. R. Montgomery (1999), Effects of hydraulic roughness on surface textures of gravel-bed rivers, *Water Resour. Res.*, *35*(11), 3507–3521, doi:10.1029/1999WR900138.

Buffington, J. M., D. R. Montgomery, and H. M. Greenberg (2004), Basin-scale availability of salmonid spawning gravel as influenced by channel type and hydraulic roughness in mountain catchments, *Can. J. Fish. Aquat. Sci.*, *61*(11), 2085–2096, doi:10.1139/f04-141.

Byrd, T. C., D. J. Furbish, and J. Warburton (2000), Estimating depth-averaged velocities in rough channels, *Earth Surf. Processes Landforms*, *25*(2), 167–173.

Cao, H. H. (1985), *Resistance hydraulique d'un lit à gravier mobile à pente raide; étude expérimentale*, 285 pp., Ecole Polytech. Fed. de Lausane, Lausanne, Switzerland.

Carling, P. A., M. Hoffmann, A. A. Blatter, and A. Dittrich (2002), Drag of emergent and submerged rectangular obstacles in turbulent flow above bedrock surface, in *Rock Scour due to Falling High-Velocity Jets*, edited by A. J. Schleiss, and E. Bollaert, pp. 83–94, Swets and Zeitlinger, Lisse, Netherlands.

Carollo, F. G., V. Ferro, and D. Termini (2005), Analyzing turbulence intensity in gravel bed channels, *J. Hydraul. Eng.*, *131*(12), 1050–1061, doi:10.1061/(ASCE)0733-9429(2005)131:12(1050).

Chan, H. C., W. C. Huang, J. M. Leu, and C. J. Lai (2007), Macroscopic modeling of turbulent flow over a porous medium, *Int. J. Heat Fluid Flow*, *28*(5), 1157–1166, doi:10.1016/j.ijheatfluidflow.2006.10.005.

Chaplin, J. R., and P. Teigen (2003), Steady flow past a vertical surface-piercing circular cylinder, *J. Fluids Struct.*, *18*(3–4), 271–285, doi:10.1016/j.jfluidstructs.2003.07.009.
Chaudhary, K., M. B. Cardenas, W. Deng, and P. C. Bennett (2011), The role of eddies inside pores in the transition from Darcy to Forchheimer flows, *Geophys. Res. Lett.*, *38*, L24405, doi:10.1029/2011GL050214.
Cheng, N.-S., X. Liu, X. Chen, and C. Qiao (2016), Deviation of permeable coarse-grained boundary resistance from Nikuradse's observations, *Water Resour. Res.*, *52*, 1194–1207, doi:10.1002/2015WR017666.
Chow, V. T. (1959), *Open Channel Hydraulics*, 680 pp., McGraw-Hill, New York.
Christensen, B. A. (1972), Incipient motion on cohesionless channel banks, in *Sedimentation: Symposium to Honor Professor H.A. Einstein*, edited by H. S. Shen, pp. 1–22, Colo. State Univ., Fort Collins.
Church, M., M. A. Hassan, and J. F. Wolcott (1998), Stabilizing self-organized structures in gravel-bed stream channels: Field and experimental observations, *Water Resour. Res.*, *34*(11), 3169–3179.
Coleman, S. E., V. I. Nikora, S. R. McLean, and E. Schlicke (2007), Spatially averaged turbulent flow over square ribs, *J. Eng. Mech.*, *133*(2), 194–204, doi:10.1061/(ASCE)0733-9399(2007)133:2(194).
Cooper, J. R., J. Aberle, K. Koll, and S. J. Tait (2013), Influence of relative submergence on spatial variance and form-induced stress of gravel-bed flows, *Water Resour. Res.*, *49*, 5765–5777, doi:10.1002/wrcr.20464.
Crowe, J. C. (2002), An experimental study of the step pool bed form, PhD dissertation, 164 pp., Johns Hopkins Univ., Baltimore, Md.
Defina, A., and A. C. Bixio (2005), Mean flow and turbulence in vegetated open channel flow, *Water Resour. Res.*, *41*, W07006, doi:10.1029/2004WR003475.
Dittrich, A., and K. Koll (1997), Velocity field and resistance of flow over rough surfaces with large and small relative roughness, *Int. J. Sediment Res.*, *12*(3), 21–33.
Einstein, H. A., and N. L. Barbarossa (1952), River channel roughness, *Trans. Am. Soc. Civ. Eng.*, *117*, 1121–1146.
Engelund, F., and E. Hansen (1967), *A Monograph on Sediment Transport in Alluvial Streams*, Danish Tech. Press, Copenhagen.
Ferguson, R. (2007), Flow resistance equations for gravel- and boulder-bed streams, *Water Resour. Res.*, *43*, W05427, doi:10.1029/2006WR005422.
Ferguson, R. I. (2012), River channel slope, flow resistance, and gravel entrainment thresholds, *Water Resour. Res.*, *48*, W05517, doi:10.1029/2011WR010850.
Ferro, V. (2003), Flow resistance in gravel-bed channels with large-scale roughness, *Earth Surf. Processes Landforms*, *28*(12), 1325–1339, doi:10.1002/esp.589.
Flammer, G. H., J. P. Tullis, and E. S. Mason (1970), Free surface, velocity gradient flow past hemisphere, *J. Hydraul. Div. Am. Soc. Civ. Eng.*, *7*, 1485–1502.
Ghisalberti, M. (2009), Obstructed shear flows: Similarities across systems and scales, *J. Fluid Mech.*, *641*, 51–61, doi:10.1017/S0022112009992175.
Ghisalberti, M., and H. Nepf (2009), Shallow flows over a permeable medium: The hydrodynamics of submerged aquatic canopies, *Transp. Porous Media*, *78*(3), 385–402, doi:10.1007/s11242-009-9434-x.
Gioia, G., and P. Chakraborty (2006), Turbulent friction in rough pipes and the energy spectrum of the phenomenological theory, *Phys. Rev. Lett.*, *96*(4), 044502, doi:10.1103/PhysRevLett.96.044502.
Goring, D. G., and V. I. Nikora (2002), Despiking acoustic Doppler velocimeter data, *J. Hydraul. Eng.*, *128*(1), 117–126, doi:10.1061/(ASCE)0733-9429(2002)128:1(117).
Hay, A. D. (1947), Flow about semi-submerged cylinders of finite length, report, 174 pp., Princeton Univ., Princeton, N. J.
Heimann, F. U. M., D. Rickenmann, J. M. Turowski, and J. W. Kirchner (2015), SedFlow—A tool for simulating fractional bedload transport and longitudinal profile evolution in mountain streams, *Earth Surf. Dyn.*, *3*(1), 15–34, doi:10.5194/esurf-3-15-2015.
Huthoff, F., D. C. M. Augustijn, and S. Hulscher (2007), Analytical solution of the depth-averaged flow velocity in case of submerged rigid cylindrical vegetation, *Water Resour. Res.*, *43*, W06413, doi:10.1029/2006WR005625.
Islam, M. R., and D. Z. Zhu (2013), Kernel density-based algorithm for despiking ADV data, *J. Hydraul. Eng.*, *139*(7), 785–793, doi:10.1061/(ASCE)HY.1943-7900.0000734.
Kamphuis, J. W. (1974), Determination of sand roughness for fixed beds, *J. Hydraul. Res.*, *12*(2), 193–202.
Katul, G., P. L. Wiberg, J. Albertson, and G. Hornberger (2002), A mixing layer theory for flow resistance in shallow flows, *Water Resour. Res.*, *38*(11), 1250, doi:10.1029/2001WR000817.
Kean, J. W., S. W. McCoy, G. E. Tucker, D. M. Staley, and J. A. Coe (2013), Runoff-generated debris flows: Observations and modeling of surge initiation, magnitude, and frequency, *J. Geophys. Res. Earth Surf.*, *118*, 2190–2207, doi:10.1002/jgrf.20148.
Klopstra, D., H. J. Barneveld, J. M. Van Noortwijk, and E. H. van Velzen (1997), Analytical model for hydraulic roughness of submerged vegetation, in *Managing Water: Coping With Scarcity and Abundance*, pp. 775–780, Am. Soc. of Civ. Eng., Reston, Va.
Konings, A. G., G. G. Katul, and S. E. Thompson (2012), A phenomenological model for the flow resistance over submerged vegetation, *Water Resour. Res.*, *48*, W02522, doi:10.1029/2011WR011000.
Lamb, M. P., W. E. Dietrich, and J. G. Venditti (2008), Is the critical shields stress for incipient sediment motion dependent on channel-bed slope?, *J. Geophys. Res.*, *113*, F02008, doi:10.1029/2007JF000831.
Lawrence, D. S. L. (1997), Macroscale surface roughness and frictional resistance in overland flow, *Earth Surf. Processes Landforms*, *22*(4), 365–382.
Lawrence, D. S. L. (2000), Hydraulic resistance in overland flow during partial and marginal surface inundation: Experimental observations and modeling, *Water Resour. Res.*, *36*(8), 2381–2393.
Lenzi, M. A., V. D'Agostino, and P. Billi (1999), Bedload transport in the instrumented catchment of the Rio Cordon. Part 1: Analysis of bedload records, conditions and threshold of bedload movement, *Catena*, *36*, 171–190.
Manes, C., D. Pokrajac, and I. McEwan (2007), Double-averaged open-channel flows with small relative submergence, *J. Hydraul. Eng.*, *133*(8), 896–904, doi:10.1061/(ASCE)0733-9429(2007)133:8(896).
Manes, C., D. Poggi, and L. Ridolfi (2011a), Turbulent boundary layers over permeable walls: Scaling and near-wall structure, *J. Fluid Mech.*, *687*, 141–170, doi:10.1017/jfm.2011.329.
Manes, C., D. Pokrajac, V. I. Nikora, L. Ridolfi, and D. Poggi (2011b), Turbulent friction in flows over permeable walls, *Geophys. Res. Lett.*, *38*, L03402, doi:10.1029/2010GL045695.
Manes, C., L. Ridolfi, and G. Katul (2012), A phenomenological model to describe turbulent friction in permeable-wall flows, *Geophys. Res. Lett.*, *39*, L14403, doi:10.1029/2012GL052369.
Meyer-Peter, E., and R. Müller (1948), Formulas for bed-load transport, in *Proceedings of the 2nd Congress, International Association of Hydraulic Research*, pp. 39–64, Int. Assoc. Hydraul. Res., Delft, Netherlands.
Millar, R. G. (1999), Grain and form resistance in gravel-bed rivers, *J. Hydraul. Res.*, *37*(3), 303–312.
Mizuyama, T. (1977), Bedload transport in steep channels, PhD dissertation, 118 pp., Kyoto Univ., Kyoto, Japan.

Mueller, E. R., J. Pitlick, and J. Nelson (2005), Variation in the reference shields stress for bed load transport in gravel-bed streams and rivers, *Water Resour. Res.*, *41*, W04006, doi:10.1029/2004WR003692.
Nelson, J., W. W. Emmett, and J. D. Smith (1991), Flow and sediment transport in rough channels, in *Proceedings of the 5th Interagency Sedimentation Conference*, edited by S.-S. Fan and Y.-H. Kuo, pp. 55–62, Dept. of Energy, Printed by Federal Energy Regulatory Commission, Washington D. C.
Nepf, H., M. Ghisalberti, B. White, and E. Murphy (2007), Retention time and dispersion associated with submerged aquatic canopies, *Water Resour. Res.*, *43*, W04422, doi:10.1029/2006WR005362.
Nepf, H. M. (2012), Hydrodynamics of vegetated channels, *J. Hydraul. Res.*, *50*(3), 262–279, doi:10.1080/00221686.2012.696559.
Nepf, H. M., and E. R. Vivoni (2000), Flow structure in depth-limited, vegetated flow, *J. Geophys. Res.*, *105*(C12), 28,547–28,557, doi:10.1029/2000JC900145.
Nezu, I., and H. Nakagawa (1993), *Turbulence in Open-Channel Flows*, 281 pp., A. A. Balkema, Rotterdam, Netherlands.
Nezu, I., and W. Rodi (1986), Open-channel flow measurements with a laser Doppler anemometer, *J. Hydraul. Eng.*, *112*(5), 335–355.
Nikora, V., and D. Goring (2000), Flow turbulence over fixed and weakly mobile gravel beds, *J. Hydraul. Eng.*, *126*(9), 679–690.
Nikora, V., D. Goring, I. McEwan, and G. Griffiths (2001), Spatially averaged open-channel flow over rough bed, *J. Hydraul. Eng.*, *127*(2), 123–133.
Nikora, V., K. Koll, I. McEwan, S. McLean, and A. Dittrich (2004), Velocity distribution in the roughness layer of rough-bed flows, *J. Hydraul. Eng.*, *130*(10), 1036–1042.
Nikora, V. I., D. G. Goring, and B. J. F. Biggs (1998), On gravel-bed roughness characterization, *Water Resour. Res.*, *34*(3), 517–527, doi:10.1029/97WR02886.
Nikuradse, J. (1933), Stromungsgesetze in rauhen rohren, *Forschg. Arb. Ing. Wes.*, *361*, 22.
Nitsche, M., D. Rickenmann, J. M. Turowski, A. Badoux, and J. W. Kirchner (2011), Evaluation of bedload transport predictions using flow resistance equations to account for macro-roughness in steep mountain streams, *Water Resour. Res.*, *47*, W08513, doi:10.1029/2011WR010645.
Nowell, A. R. M., and M. Church (1979), Turbulent flow in a depth-limited boundary layer, *J. Geophys. Res.*, *88*(C8), 4816–4824.
Packman, A., M. Salehin, and M. Zaramella (2004), Hyporheic exchange with gravel beds: Basic hydrodynamic interactions and bedform-induced advective flows, *J. Hydraul. Eng.*, *130*(7), 647–656, doi:10.1061/(ASCE)0733-9429(2004)130:7(647).
Parker, G. (1991), Selective sorting and abrasion of river gravel. II: Applications, *J. Hydraul. Eng.*, *117*(2), 150–171.
Parker, G., and A. W. Peterson (1980), Bar resistance of gravel-bed streams, *J. Hydraul. Div. Am. Soc. Civ. Eng.*, *106*, 1559–1575.
Prancevic, J. P., and M. P. Lamb (2015a), Particle friction angles in steep mountain channels, *J. Geophys. Res. Earth Surf.*, *120*, 242–259, doi:10.1002/2014JF003286.[10.1002/2014JF003286]
Prancevic, J. P., and M. P. Lamb (2015b), Unraveling bed slope from relative roughness in initial sediment motion, *J. Geophys. Res. Earth Surf.*, *120*, 474–489, doi:10.1002/2014JF003323.
Prancevic, J. P., M. P. Lamb, and B. M. Fuller (2014), Incipient sediment motion across the river to debris-flow transition, *Geology*, *42*(3), 191–194, doi:10.1130/G34927.1.
Rathnayake, U., and N. Izumi (2009), Theoretical analysis for the interaction between the river flow and the seepage flow, in *Proceedings of the 6th International Conference on Fluid Mechanics*, pp. 46–51, World Scientific and Engineering.
Raupach, M. R., R. A. Antonia, and S. Rajagopalan (1991), Rough-wall turbulent boundary layers, *Appl. Mech. Rev.*, *44*(1), 1–25.
Recking, A. (2009), Theoretical development on the effects of changing flow hydraulics on incipient bed load motion, *Water Resour. Res.*, *45*, W04401, doi:10.1029/2008WR006826.
Recking, A., P. Frey, A. Paquier, P. Belleudy, and J. Y. Champagne (2008a), Feedback between bed load transport and flow resistance in gravel and cobble bed rivers, *Water Resour. Res.*, *44*, W05412, doi:10.1029/2007WR006219.
Recking, A., P. Frey, A. Paquier, P. Belleudy, and J. Y. Champagne (2008b), Bed-load transport flume experiments on steep slopes, *J. Hydraul. Eng.*, *134*(9), 1302–1310, doi:10.1061/(ASCE)0733-9429(2008)134:9(1302).
Rice, C. E., K. C. Kadavy, and K. M. Robinson (1998), Roughness of loose rock riprap on steep slopes, *J. Hydraul. Eng.*, *124*(2), 179–185, doi:10.1061/(ASCE)0733-9429(1998)124:2(179).
Rickenmann, D. (2001), Comparison of bed load transport in torrents and gravel bed streams, *Water Resour. Res.*, *37*(12), 3295–3305, doi:10.1029/2001WR000319.
Rickenmann, D. (2012), Alluvial steep channels: Flow resistance, bedload transport and transition to debris flows, in *Gravel Bed Rivers: Processes, Tools, Environment*, edited by P M. Church, P. Biron, and A. Roy, pp. 386–397, John Wiley, Chichester, U. K.
Rickenmann, D., and A. Recking (2011), Evaluation of flow resistance in gravel-bed rivers through a large field data set, *Water Resour. Res.*, *47*, W07538, doi:10.1029/2010WR009793.
Rowinski, P. M., and J. Kubrak (2002), A mixing-length model for predicting vertical velocity distribution in flows through emergent vegetation, *Hydrol. Sci. J.*, *47*(6), 893–904, doi:10.1080/02626660209492998.
Scheingross, J. S., E. W. Winchell, M. P. Lamb, and W. E. Dietrich (2013), Influence of bed patchiness, slope, grain hiding, and form drag on gravel mobilization in very steep streams, *J. Geophys. Res. Earth Surf.*, *118*, 982–1001, doi:10.1002/jgrf.20067.
Schlichting, H. (1979), *Boundary-Layer Theory*, 7th ed., 535 pp., McGraw-Hill, New York.
Schneider, J. M., D. Rickenmann, J. M. Turowski, and J. W. Kirchner (2015a), Self-adjustment of stream bed roughness and flow velocity in a steep mountain channel, *Water Resour. Res.*, *51*, 7838–7859, doi:10.1002/2015WR016934.
Schneider, J. M., D. Rickenmann, J. M. Turowski, K. Bunte, and J. W. Kirchner (2015b), Applicability of bed load transport models for mixed-size sediments in steep streams considering macro-roughness, *Water Resour. Res.*, *51*, 5260–5283, doi:10.1002/2014WR016417.
Straub, L. G., and O. P. Lamb (1956), Studies of air entrainment on open-channel flows, *Am. Soc. Civ. Eng. Trans.*, *121*, 30–44.
Vafai, K., and S. J. Kim (1990), Fluid-mechanics of the interface region between a porous-medium and a fluid layer—An exact solution, *Int. J. Heat Fluid Flow*, *11*(3), 254–256, doi:10.1016/0142-727X(90)90045-D.
Valle, B. L., and G. B. Pasternack (2006), Air concentrations of submerged and unsubmerged hydraulic jumps in a bedrock step-pool channel, *J. Geophys. Res.*, *111*, F03016, doi:10.1029/2004JF000140.
Wang, J., C. K. Chen, Z. N. Dong, and X. Zhenhuan (1993), The effects of bed roughness on the distribution of turbulent intensities in open-channel flow, *J. Hydraul. Res.*, *31*(1), 89–98.
Wang, J., Z. D. Jin, R. G. Hilton, F. Zhang, A. L. Densmore, G. Li, and A. J. West (2015), Controls on fluvial evacuation of sediment from earthquake-triggered landslides, *Geology*, *43*(2), 115–118, doi:10.1130/G36157.1.
White, B. L., and H. M. Nepf (2008), A vortex-based model of velocity and shear stress in a partially vegetated shallow channel, *Water Resour. Res.*, *44*, W01412, doi:10.1029/2006WR005651.

Wiberg, P. L., and D. M. Rubin (1989), Bed roughness produced by saltating sediment, *J. Geophys. Res.*, *94*(C4), 5011–5016, doi:10.1029/JC094iC04p05011.

Wiberg, P. L., and J. D. Smith (1987a), Initial motion of coarse sediment in streams of high gradient, in Erosion and Sedimentation in the 1033 Pacific Rim (Proceedings of the Corvallis Symposium), IAHS Publ. 165, pp. 299–308, International Association of Hydrological Sciences (IAHS).

Wiberg, P. L., and J. D. Smith (1987b), Calculations of the critical shear stress for motion of uniform and heterogeneous sediments, *Water Resour. Res.*, *23*(8), 1471–1480.

Wiberg, P. L., and J. D. Smith (1991), Velocity distribution and bed roughness in high gradient streams, *Water Resour. Res.*, *27*(5), 825–838.

Wilcox, A. C., J. M. Nelson, and E. E. Wohl (2006), Flow resistance dynamics in step-pool channels: 2. Partitioning between grain, spill, and woody debris resistance, *Water Resour. Res.*, *42*, W05419, doi:10.1029/2005WR004278.

Wohl, E. E., and D. M. Thompson (2000), Velocity characteristics along a small step-pool channel, *Earth Surf. Processes Landforms*, *25*, 353–367.

Yager, E. M., J. W. Kirchner, and W. E. Dietrich (2007), Calculating bed load transport in steep boulder bed channels, *Water Resour. Res.*, *43*, W07418, doi:10.1029/2006WR005432.

Yager, E. M., W. E. Dietrich, J. W. Kirchner, and B. W. McArdell (2012), Prediction of sediment transport in step-pool channels, *Water Resour. Res.*, *48*, W01541, doi:10.1029/2011WR010829.

Zhou, D. H., and C. Mendoza (1993), Flow through porous bed of turbulent stream, *J. Eng. Mech.*, *119*(2), 365–383, doi:10.1061/(ASCE)0733-9399(1993)119:2(365).

Zimmermann, A. (2010), Flow resistance in steep streams: An experimental study, *Water Resour. Res.*, *46*, W09536, doi:10.1029/2009WR007913.

Zimmermann, A., M. Church, and M. A. Hassan (2010), Step-pool stability: Testing the jammed state hypothesis, *J. Geophys. Res.*, *115*, F02008, doi:10.1029/2009JF001365.